The International Journal of Advanced Manufacturing Technology
https://doi.org/10.1007/s00170-022-09074-7

ORIGINAL ARTICLE

Correlation assessment and modeling of intra-axis errors of prismatic axes for CNC machine tools

Ahlem Mechta[1] · Mohamed Slamani[1,2] · Moussa Zaoui[1] · René Mayer[3] · Jean-François Chatelain[2]

Received: 27 December 2021 / Accepted: 16 March 2022

Abstract
This paper presents an experimental study conducted to assess the correlation between the intra-axis errors of prismatic axes for CNC machine tools. The validity and reliability of parametric models for the modeling of intra-axis errors (IAEs) of CNC machine tools in the context of indirect calibration are also assessed in this work. Three CNC machine tools with various controllers and guidance technologies were tested using two different measuring instruments. Two predictive models, namely Bézier and B-spline curves, are described and compared for the first time in this work. Both models are experimentally evaluated for accuracy and predictive efficiency using four evaluation criteria and new data sets from the three tested CNC machine tools. Results show a strong correlation between the positioning errors and the pitch and yaw errors for all the tested machines. The results also show that both proposed models are appropriate for the modeling of intra-axis errors, with the B-spline curves coming slightly on top in terms of performance. Moreover, with the same number of control points ($n=5$), the two models provide residuals that are lower than the repeatability of the machine for most intra-axis errors tested. This experimental study thus confirms that a Bézier model of degree four and a B-spline model of degree two, both with five control points, are sufficient to represent the intra-axis errors for the tested CNC machine tools.

Keywords Machine tool · Intra-axis errors · Correlation · Bézier model · B-spline model

1 Introduction

Industry is quickly moving towards ever more precise and intelligent manufacturing [1]. Precise and intelligent machine tools play an important role in the success of smart factory concept in the aerospace industry [2]. The challenge continuing to face this strategic sector, though, is how to produce parts of high quality while minimizing the working time and manufacturing costs [3]. However, even if the machine tool is sufficiently precise during installation, its performance may gradually degrade over time due to the intensity of the work to which it is subjected, which causes wear and tear in the machine subsystems [4]; this in turn leads to an increase in the volume of Abbé errors [5]. Furthermore, the degradation of the linear axes leads to the amplification of intra-axis errors [6]. In such an environment, the characterization and assessment of machine tool performance is crucial.

Despite the technological advances that have occurred both in machine tools and in their control systems, many factors still hamper the performance of these machines in terms of precise machining [7], including geometric and kinematic errors [8], thermal errors [9], servo errors [10], and errors induced by the cutting force [11]. Geometric errors represent some of the greatest sources of inaccuracy in machine tools [12, 13] and are themselves caused by factors such as imperfect geometries of guideways, carriages, beds, and lead screws, and their misalignment in the machine structure [14]. They generally vary slowly over time but can be affected more rapidly by the thermal error and dynamic loading [15]. These errors are systematic in nature [16, 17]. In particular, intra-axis errors (IAEs), which are deviations from the nominal motion of a machine axis, are not constant [18], but instead, vary according to the nominal position of the moving mechanical axis [19].

✉ Mohamed Slamani
mohamed.slamani@univ-msila.dz

[1] MMS Lab, Faculty of Technology, University of M'sila, M'Sila, Algeria

[2] Mechanical Engineering Department, École de technologie supérieure, Montreal, Canada

[3] Mechanical Engineering Department, École Polytechnique de Montréal, Montreal, Canada

Published online: 26 March 2022

In the context of indirect calibration and simulation of volumetric errors, i.e., the location error to the tool with respect to the work piece, intra-axis errors have been modeled by polynomials in several research works [20–28]. However, the main disadvantage with polynomial modeling is its inflexibility. Moreover, the polynomial models lend themselves to very limited extrapolation. These disadvantages limit the use of polynomial models for modeling geometric errors of CNC machine tools for precision machining applications in the context of smart factory. Therefore, robust and reliable models are still required to meet the challenges faced by industry.

Several recent research works have shown that parametric curves such as Bézier [29, 30], B-splines [31, 32], and NURBS [33] constitute the most popular interpolation techniques for CNC systems. Their benefits outweigh those of polynomials in terms of flexibility, and they allow the user great freedom when it comes to controlling the shape of the final curve. Additionally, they enable the separation of variables as well as direct calculations point coordinates. Furthermore, using parametric curves in CNC machine tool interpolators can lead to reduced machining time, better precision, and improved surface finish [34]. As well, such curves can also provide smooth tool paths to control the dynamic behavior of the machine tool [35].

A recursive compensation strategy was proposed by Khan and Chen [36] for systematic geometric error compensation on five-axis machine tools and inverse technique was implemented to find the corrected positions of prismatic and rotary joints. They modeled geometric errors by a cubic spline function. The pose errors in volumetric workplace were calculated based on the forward kinematics approach, whereas the inverse kinematics technique was used to detect the corrected motions of the joints for compensating this error through software. More recently, a path planning algorithm for curvature adapted CNC machining of freeform surfaces was proposed by Bartoň et al. [37]. Their work was based on a careful geometric analysis of curvature-adapted machining via so-called second order line contact between tool and target surface. The tilt angle of the tool was represented as a cubic B-spline function over a uniform knot sequence. In a similar context, Lartigue et al. [38] found that polynomial formats of tool trajectories are well adapted to high speed machining of free-form surfaces. An algorithm for flank CNC machining of general, doubly curved, free-form surfaces was proposed by Calleja et al. [39]. To generate a ruled surface that represents a single continuous sweep of a rigid conical milling tool, a spline surface fitting is used in their study. Then, their approach was validated by comparing the results of their proposed algorithm with two industrial benchmark models. They claimed that their proposed algorithm outperform the commercial software in terms of the approximation error in cases where the patches are roughly of the same area.

Notwithstanding the aforementioned advantages, the use of parametric models in the modeling of intra-axis errors is quite limited. Furthermore, up to now, no research has been conducted to choose the optimal number of control points required to represent each intra-axis error. In this work, the parametric modeling approach is used in modeling the intra-axis errors of CNC machine tools. Accordingly, Bézier and B-spline curves are investigated as alternative models to replace polynomial curves in the indirect calibration procedure.

The intra-axis motion errors of each axis can be described by six degrees of freedom: three translations and three rotations [40], whereas ideally, only one degree of freedom is present along the axis of the desired movement that it is linear or of rotation [41]. In other words, the six degrees of freedom (the six intra-axis errors) come from the same source, i.e., the moving axis physical sub-systems. A correlation may exist between these intra-axis errors. However, most existing works in this area focus on the relationship between straightness and angular errors [12, 42, 43]. Rotational error components contribute more to the machine's positioning errors than straightness errors due to the Abbe error [44, 45]. Testing the significance of correlation between the different intra-axis errors is crucial when it comes to the fast calibration and modeling of machine tool errors. Detecting a significance of correlation can lead to a significant reduction in the machine tool error model by omitted certain redundant or correlated errors and hence yields a more reliable estimation of the remaining parameters in the machine tool error model during the calibration process [44]. In spite of its importance, testing the significance of correlation between the different intra-axis errors on an experimental and statistical basis was not evaluated in a rigorous way. In this paper, a statistical analysis-based comparative study is carried out in order to validate the assumption concerning the correlation between the intra-axis errors of the same axis.

The main objective of this work is therefore to provide machine tool designers, manufacturers, and users with new tools for improving the quality of machines, by quantifying the correlation between different intra-axis errors and by exploiting the opportunities offered by parametric models such as Bézier and B-spline curves. In the proposed approach, data on the intra-axis errors of the three prismatic axes of a CNC machine tool are collected through a laser interferometer and are then used to the modeling of the intra-axis errors. The collected data are also used to better understand how these errors correlate.

This study is broken down into the following sub-objectives:

– Perform bidirectional tests for the intra-axis errors for each prismatic axis of the machine using two different measurement devices;

- Perform a statistical analysis for the positioning repeatability, accuracy, and reproducibility of results;
- Evaluate the correlation between intra-axis errors;
- Choose the optimum degree and the optimal number of control points for each measured intra-axis error;
- Evaluate backlash errors;
- Evaluate the ability to extrapolate the models to other types of machines with various control and guidance technologies;
- Evaluate the adequacy of the proposed models.

This work therefore covers two distinct and complementary aspects of machine tool metrology. The first helps to better understand and interpret the relationships between intra-axis errors and provides new industrial contribution by implementing new tools for analyzing and predicting the performance of machine tools for and by machine tool users. The second provides new research knowledge to improve the state of the art in the modeling of CNC machine tool errors.

The remainder of the paper is organized as follows: Sect. 2 describes the mathematical tools and the statistical criteria that are used to build and evaluate the proposed models. Section 3 describes the experimental procedures. The results and discussion are presented in Sect. 4, and finally, the conclusion is given in Sect. 5.

2 Modeling approach

Bézier and B-spline forms are among the most important tools used for modeling curves and surfaces in CAD/CAM. Given their advantages presented above, Bézier and B-Spline curves are used in this study.

(a) Bézier model

Bézier functions are important tools used for modeling smooth curves. A Bézier curve of degree n is a parametric curve specified by $n+1$ points, defining the Bézier control polygon. The basis functions used in the Bézier interpolation are Bernstein polynomials [46] defined by:

$$B_i^n(t) = \binom{n}{i} t^i (1-t)^{n-i} \tag{1}$$

where:

$$\binom{n}{i} = \begin{cases} \frac{n!}{i!(n-i)!} & if \ \ 0 \le i \le n \\ 0 & else \end{cases} \tag{2}$$

The parameter t is in the range [0, 1] and there are $n+1$ polynomials defined for each i from 0 to n. The Bézier curve with respect to the Bernstein basis is thus defined in the interval [0, 1] as:

$$b(t) = \sum_{i=0}^{n} P_i B_i^n(t) \tag{3}$$

where P_i are the control points defining the Bézier polygon.

(b) B-spline model

A B-spline curve (S (t)) is defined by:

$$S(t) = \sum_{i=0}^{n} P_i N_{i,K}(t) \tag{4}$$

where $N_{i,K}(t)$ is the *Kth* degree B-spline basis function defined on a nonperiodic and uniform knot vector and P_i are the control points [47]. t is the parametric coordinates ranged within [0, 1].

$$N_{i,K} = \begin{cases} 1 \ if \ \ t \in [t_i, t_{i+1}) \\ 0 \quad otherwise \end{cases}$$

and

$$N_{i,K}(t) = \left(\frac{t - t_i}{t_{i+K+1} - t_i}\right) N_{i,K-1}(t) + \left(\frac{t_{i+K} - t}{t_{i+K} - t_{i+1}}\right) N_{i+1,K-1}(t) \tag{5}$$

$[t_i, \ldots, t_{i+K}]$ is the knot vector, and the parameter t ranged within the interval $[t_{K+1}, t_{n+1}]$.

(c) Methodology of modeling and selection criteria

In this modeling approach, the terms and the control points (Eqs. (3) and (4)) are introduced successively, but before any introduction of a new term or additional control point, the adequacy of the model is tested.

During the modeling process, it is interesting to examine the relationship between observed data and predicted values. One approach is to examine what happens when the proposed model does not fit the observed data exactly, i.e., to analyze the residuals. Residuals are mainly analyzed to test the validity of a model and to detect its failures. The decision rule adopted in the present study is to favor the model if the residual varies within a tolerance band that is less than or equal to the axis positioning repeatability. Then, no term or control points can be added to the model. If not, the model is rejected. In this case, a new term or a new control point has to be added to the model and the same procedure is followed until the selection criterion is satisfied (residual less than repeatability).

The residual in our case is defined as the difference between the average of the observed values and the values estimated by the model. It has the particularity of representing the part that is not explained by the model. It is commonly noted as follows:

$$e_i = \overline{Y}_i - \hat{Y}_i \tag{6}$$

where:

$\overline{Y}_i$ is the average of the intra-axis error at position i; and

$\hat{Y}_i$ is the estimated model at position i.

For each axis of the tested machine, the positioning repeatability and the accuracy are calculated according to ISO 230–2 [48].

$$R_i = max\left[2S_i \uparrow +2S_i \downarrow +\left|B_i\right|;R_i \uparrow ;R_i \downarrow\right] \tag{7}$$

where: $R_i \uparrow = 4S_i \uparrow$ and $R_i \downarrow = 4S_i \downarrow$;

R_i is the bidirectional positioning repeatability;

B_i is the backlash;

i represents the target positions;

$R_i \uparrow$ is the unidirectional positioning repeatability for the forward direction; and

$R_i \downarrow$ is the unidirectional positioning repeatability for the backward direction.

The standard deviation for the forward and the backward directions can be calculated by the following formulas:

$$S_i \downarrow = \sqrt{\frac{1}{n-1}\sum_{j=1}^{n}\left(Y_{ij} \downarrow -\overline{Y}_i \downarrow\right)} \tag{8}$$

$$S_i \uparrow = \sqrt{\frac{1}{n-1}\sum_{j=1}^{n}\left(Y_{ij} \uparrow -\overline{Y}_i \uparrow\right)} \tag{9}$$

and $n \geq 3$

The bidirectional accuracy is:

$$A = max\left[\overline{Y}_i \uparrow +2S_i \uparrow ;\overline{Y}_i \downarrow +2S_i \downarrow\right] - min\left[\overline{Y}_i \uparrow -2S_i \uparrow ;\overline{Y}_i \downarrow -2S_i \downarrow\right] \tag{10}$$

The difference between the average of the intra-axis errors for the forward direction ($\overline{Y}_i \uparrow$) and the backward direction ($\overline{Y}_i \downarrow$) at each target position is called the backlash. The maximum of the absolute values of the backlash at all target positions along the measured axis is the axis backlash [48].

$$B = max\left[\left|B_i\right|\right] \tag{11}$$

and

$$B_i = \overline{Y}_i \downarrow -\overline{Y}_i \uparrow \tag{12}$$

To select the most appropriate model, four statistical indicators are used. These chosen indicators are the most recommended for assessing and comparing how different models fit the same data [49]. The first indicator is the coefficient of determination (R^2):

$$R^2 = \frac{\sum_{i=1}^{n}\left(\hat{Y}_i - \overline{Y}\right)^2}{\sum_{i=1}^{n}\left(Y_i - \overline{Y}\right)^2} \tag{13}$$

where n denotes the sample size.

The second indicator is the root mean square error (RMSE):

$$RMSE = \sqrt{\frac{1}{n}\sum_{i=1}^{n}\left(\hat{Y}_i - Y_i\right)^2} \tag{14}$$

The third indicator is the mean absolute error (MAE):

$$MAE = \frac{1}{n}\sum_{i=1}^{n}\left(\left|F_i - \hat{F}_i\right|\right) \tag{15}$$

Finally, the fourth indicator is the mean absolute percentage error:

$$MAPE = \frac{100\%}{n}\sum_{i=1}^{n}\left(\left|F_i - \hat{F}_i\right| / \left|F_i\right|\right) \tag{16}$$

3 Experimental procedures

This section describes the procedures, the experimental techniques, and the materials used for the data acquisition in order to establish representative models of the intra-axis errors of the machine tool.

Calibrating a 5-axis machine tool can be a very complex, time-consuming, and expensive task, especially when machine downtime is considered. A measuring approach using 5/6D laser technology can reduce the complexity, time, and cost. 5/6D equipment can easily be used and all motion errors of an axis can be simultaneously measured from a single setup. Accordingly, two CNC machine tools were tested (Figs. 1 and 2) using 5/6D equipment manufactured by Automated Precision Inc. (API). To assess the validity of the proposed approach and the generality of the proposed models, a third machine was tested using the Renishaw laser interferometer measurement

Fig. 1 Matsuura MC.760 VX five-axis machine tool

Fig. 2 Mitsui Seiki HU40-T five-axis horizontal machining center

system (Fig. 3). With the 5/6D device, five intra-axis errors (not the roll) for each axis were measured in one setup. However, with the Renishaw laser interferometer, only the positioning errors and the two straightness errors for each axis were measured.

The types and characteristics of the three tested machines are given in Table 1.

An example of measurements along the X-axis of the Matsuura MC.760 VX machine tool using the 5/6D API instrument is illustrated in Fig. 4.

A G-code program was used to move the machine from one static position to another along a straight path across the available travel according to a linear feed move G01 instruction at a commanded feed rate of 1000 mm/min, pausing for a few seconds at each position.

Before the data acquisition was started, certain values were specified, such as the downtime ($t = 7$ s), which defines exactly when the software reads the static position of the

Fig. 3 Huron KX 8-five five-axis machining center

moving axis at each target. Furthermore, warm-up sequences were performed to reach the machine thermal steady state. These warm-up sequences were immediately followed by the data acquisition. When the first target is measured during the data acquisition process, the CNC program moves the machine to the next measuring point. After reaching the last point of the forward direction, the CNC program reverses the direction of motion and stops again at each measuring point to allow the 5/6D system to read data for the backward direction. When the starting point is reached, the first cycle is completed (Fig. 5). The machine must then pass the first measuring point to start the next cycle. This process is repeated until all the five cycles have been completed. As shown in Fig. 5, each cycle contains two travels, one for the forward direction and the other for the backward direction. The forward and backward travels allow the evaluation of the backlash for each axis.

During the laser interferometer measuring process, an overrun distance of 2 mm is used (Fig. 5) to ensure that the first and the last targets are collected in the right direction.

The methodology was implemented in a way that each linear axis of the CNC machine tool is measured separately. Therefore, for measurements taken along the X-axis, the coordinates of the axes which are not under test were $Y = -215.810$ mm, $Z = -124.540$ mm, $A = 0.0°$, and $C = 180°$. Whereas, the coordinates of the stationary axes during the measurement along the Y axis were $X = -384.664$ mm, $Z = -124.377$ mm, $A = 0.0°$, and $C = 0.0°$. Finally, when measuring along the Z-axis, the coordinates of the stationary axes were $X = -365.396$ mm, $Y = -235.435$ mm, $A = 0.0°$, and $C = 0.0°$.

4 Results and discussion

The positioning repeatability, the accuracy, and the backlash errors of the three tested machines were presented in this section. The correlation between the different intra-axis errors was also calculated and explained, followed by a comparative analysis of the two proposed models. Then, the more appropriate of the two models was selected. Tests were carried out without any kind of compensation on the controller of the machine, and thus represent the machine's physical characteristics, not numerical quantities present in the machine's compensation tables.

4.1 Analysis of the positioning repeatability, the accuracy, and the backlash errors of the three tested machines

Table 2 presents the results of the linear positioning error in terms of the bidirectional repeatability, backlash errors, and accuracy, evaluated according to ISO 230–2 [48], for

Table 1 Characteristics of the three tested machines

	Matsuura MC.760 VX Five-axis machining center	Mitsui Seiki HU40-T Five-axis machining center	Huron KX 8-five Five-axis machining center
Drive technology	Ball screw feed-drive systems	Ball screw feed-drive systems	Ball screw feed-drive systems
Controller	Yasnac MX3 controller	Fanuc 15iMa controller	Siemens 40D controller
Guiding technology	Hydrostatic bearings	Prismatic slides	Linear ball bearing slides
Travels on X/Y/Z axes	760/440 /485 [mm]	611/562/710 [mm]	650/700/450 [mm]
Measuring device used	5/6D API	5/6D API	Renishaw laser interferometer

the three axes, *X*, *Y*, and *Z*, of the three tested machines. The table shows that the Matsuura MC-760 VX machine provides the best results in terms of accuracy for the *X*- and *Y*-axes. In contrast, the Huron KX 8-five machine provides the worst results in terms of accuracy, whereas it is the most repeatable machine, and gives the fewest backlash errors among all the axes tested.

Generally, systematic errors can be compensated and decreased down to the repeatability limit, whereas random errors cannot be compensated. So, a machine with a poor accuracy and a good repeatability is always more appropriate than an accurate but less repeatable machine.

A graphical representation of the linear positioning errors of the *Z*-axis for the three tested machines is shown in Figs. 6, 7 and 8. The most important point that can be drawn from Fig. 6 is the offset between the results of the forward and the backward directions of the Matsuura machine, which can be explained by the effect of the backlash error, which exceeds 12 µm (Table 2). The results also show that this machine is still the worst in terms of backlash errors, even for the *X*- and *Y*-axes (Table 2). It should be noted that in comparison to the two other tested machines, the Matsuura MC-760 VX is the oldest one, and may be affected by wear due to its daily use, especially on the *Z*-axis exposed to gravity. On the other hand, Fig. 7 shows that the HU40 machine suffers from poor repeatability, which in some cases exceeds 8 µm (Table 2). These results remain puzzling, especially for a machine dedicated to high performance machining. The backlash of the Huron is the smallest (Fig. 8) and does not exceed 0.8 µm in the worst case (Table 2).

Fig. 4 Measuring setup on the Matsuura MC-760 VX machine tool using 5/6D API device

4.2 Assessment of the correlation between intra-axis errors

Although the six intra-axis errors of an axis are defined individually in the literature and in standards, and are modeled separately in the literature, it is interesting to analyze whether they are correlated. To assess the hypothesis of correlation, the correlation coefficient between each two intra-axis errors of each axis is calculated. The correlation coefficient provides reliable information about the strength of a linear relationship between the two assessed intra-axis errors. According to Taylor [50], a correlation coefficient in absolute value $|r| \leq 0.35$ generally represents a weak correlation. The correlation is considered modest or moderate if $|r|$ is between 0.36 and 0.67. However, if $0.68 \leq |r| \leq 0.89$, the correlation is considered strong or high, and finally, if $|r| \geq 0.9$ the correlation is considered very strong. Tables 3, 4 and 5 show the calculated correlation coefficients for each couple of intra-axis errors for the three axes of the Matsuura machine tool.

It is well known that the straightness error of a linear axis is defined as the distance between two parallel lines in the general direction of the axis, which contains exactly all the measuring points. Any slope should therefore be removed from the raw data of straightness errors.

Regarding the results of the *Y*-axis of the Matsuura machine tool, Table 3 shows that there is no correlation between the linear positioning error E_{XX} and the straightness error motion in the *Y*-axis direction (horizontal straightness error) E_{YX}. The correlation between the linear positioning error E_{XX} and the straightness error motion in the *Z*-axis direction (vertical straightness error) E_{ZX} was found modest. However, a strong correlation was observed between E_{XX} and the two angular errors, i.e., the angular error motion around the *C*-axis (yaw) E_{CX} and the angular

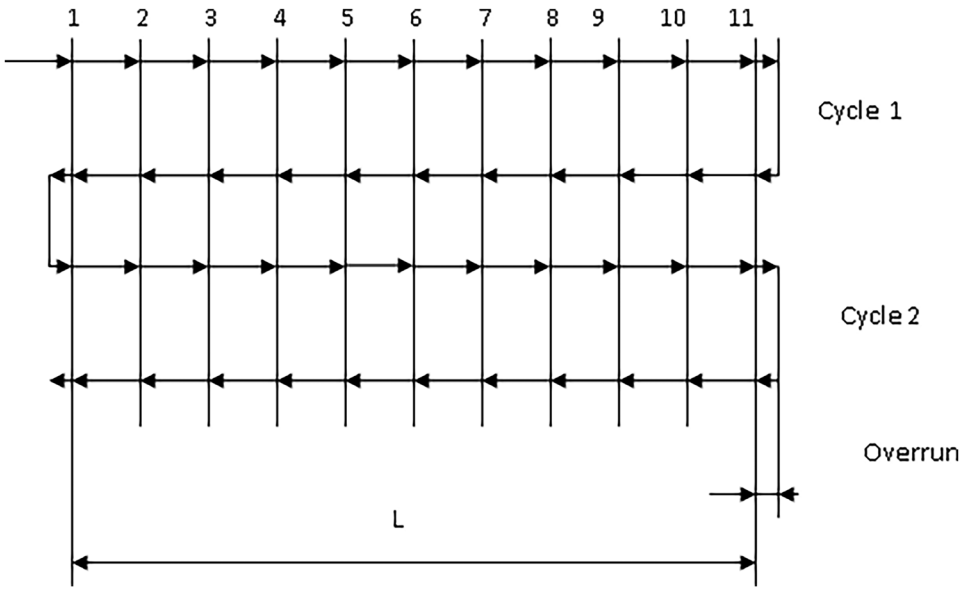

Fig. 5 Machine program summary

error motion around the *B*-axis (pitch) E_{BX}. The correlation between E_{YX} and E_{ZX} was found modest. These results also show that there is no correlation between E_{YX} and the yaw error E_{CX}. Moreover, the correlation between E_{YX} and the pitch error E_{BX} is weak. In addition, no correlation was observed between E_{ZX} and E_{BX}. The correlation between E_{CX} and E_{ZX} and E_{BX} was found respectively weak and modest.

The *Y*-axis results presented in Table 4 confirm that the correlation between the linear positioning error E_{YY} and the two angular errors E_{AY} and E_{CY} still remains strong. However, a modest correlation was observed between the straightness error E_{ZY} and the two angular errors E_{AY} and E_{CY}. The correlation between the straightness error E_{XY} and E_{YY}, E_{ZY}, E_{AY}, and E_{CY} is generally weak.

Contrary to previous observations, the results of the *Z*-axis presented in Table 5 show that there is a strong correlation between E_{XZ} and the two angular errors E_{AZ} and E_{BZ}. Moreover, Table 5 confirms yet again the strong correlation between the linear positioning error and the pitch and yaw errors. For the second time, the strong correlation between the pitch and yaw errors can be also observed.

It is commonly accepted that the three translations errors (linear positioning error and straightness errors) of machine tools can be significantly affected by the three angular errors (pitch, yaw, and roll) due to the Abbe and Bryan principles. During the measurement of the linear positioning errors with a laser interferometer, the Abbe error has a significant effect. As shown in Fig. 9a, b, the angular error motion (E_{BX}) around the *B*-axis (yaw) and the angular error motion (E_{CX}) around the *C*-axis (pitch) contribute to the linear positioning errors due to Abbe errors.

According to the Abbe principle, the linear positioning error measured by the laser interferometer system at any point in the work envelop of the machine tool can be

Table 2 Bidirectional repeatability, accuracy, and backlash errors of the linear positioning error of the three axes, *X*, *Y*, and *Z*, of the three tested machines

Machine tested	Axis	Bi-directional accuracy (μm)	Backlash (μm)	Bi-directional repeatability (μm)
Matsuura MC.760 VX	***X***	7.4	0.7	2.0
	Y	7.3	3.3	4.6
	Z	16.4	12 .1	13.3
Mitsui Seiki HU40-T	***X***	24.7	2.1	8.5
	Y	15.3	1.9	8.5
	Z	14.9	1.6	6.8
Huron KX 8-five	***X***	29.8	0.6	1.5
	Y	15.8	0.8	1.3
	Z	6.4	0.2	0.9

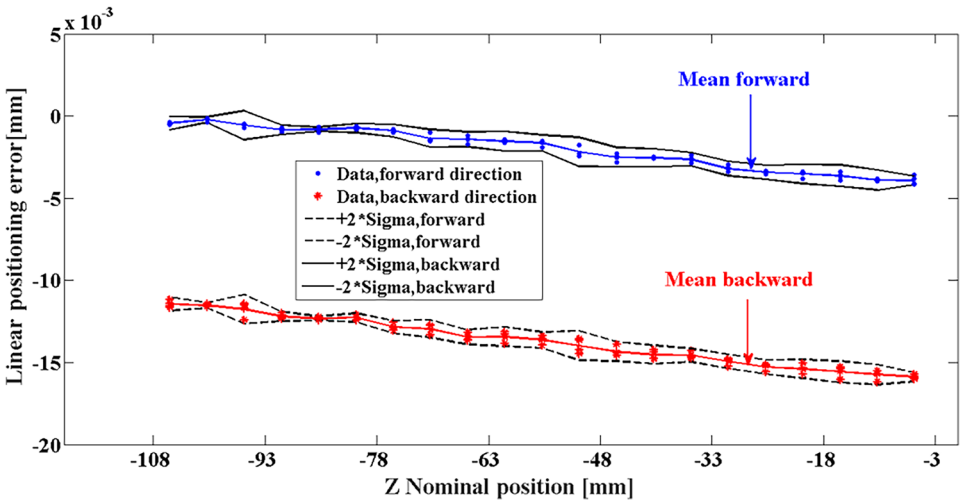

Fig. 6 Linear positioning errors, mean unidirectional and ± two unidirectional repeatability of the Z-axis of the Matsuura MC-760 VX machine

affected by angular errors, and their effects are amplified by the Abbe offset according to the following equation:

$$E_{XX} = e_{XX} - E_{CX} \times t_{ya} + E_{BX} \times t_{za} \tag{17}$$

where e_{XX} is the linear positioning error arbitrarily chosen at the ball screw level, E_{XX} is the linear positioning error measured with the laser interferometer, and t_{ya} and t_{za} are the Abbe offset in the *Y*- and *Z*-directions, respectively. Equation (17) also demonstrates the high correlation between E_{XX} and the two angular errors E_{CX} and E_{BX} shown in Table 3.

Conversely to the Abbe principle, which concerns the linear positioning errors, the Bryan principle is mainly applied on the horizontal and vertical straightness errors of machine tools. Figures 10 and 11 show the effect of the Bryan offset on the horizontal straightness error of the moving table.

The measured horizontal straightness error can be derived according to the Bryan principle as follows:

$$E_{YX} = e_{YX} + E_{CX} \times t_{xbr} - E_{AX} \times t_{zbr} \tag{18}$$

where E_{YX} is the measured horizontal straightness error and e_{YX} is the horizontal straightness error at the ball screw level.

Similarly, the measured vertical straightness error can be computed according to the Bryan principle as follows:

$$E_{ZX} = e_{ZX} - E_{BX} \times t_{xbr} + E_{AX} \times t_{ybr} \tag{19}$$

where E_{ZX} is the measured vertical straightness error and e_{ZX} is the vertical straightness error at the ball screw level. The effects of the Bryan and angular errors on the vertical straightness error are shown in Figs. 12 and 13.

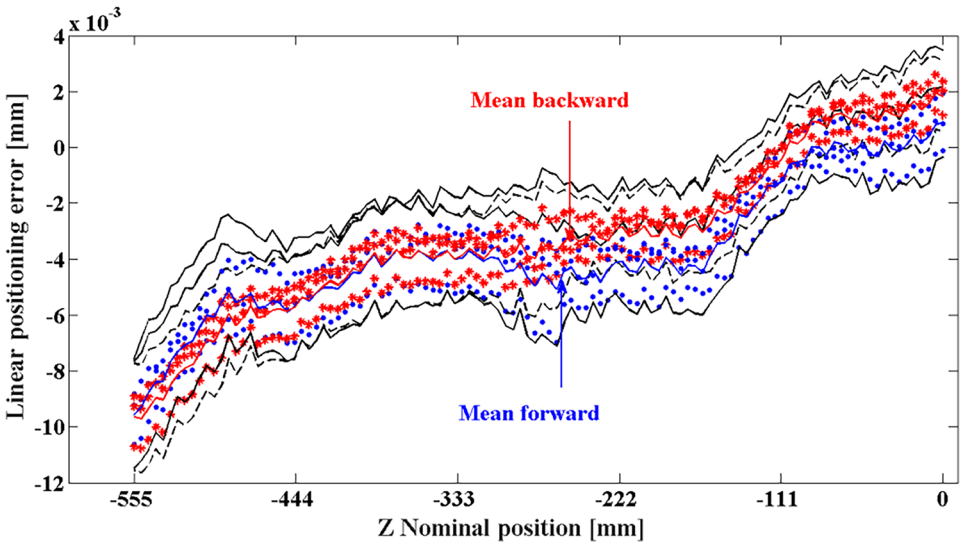

Fig. 7 Linear positioning errors, mean unidirectional and ± two unidirectional repeatability of the Z-axis of the Mitsui Seiki HU40-T machine

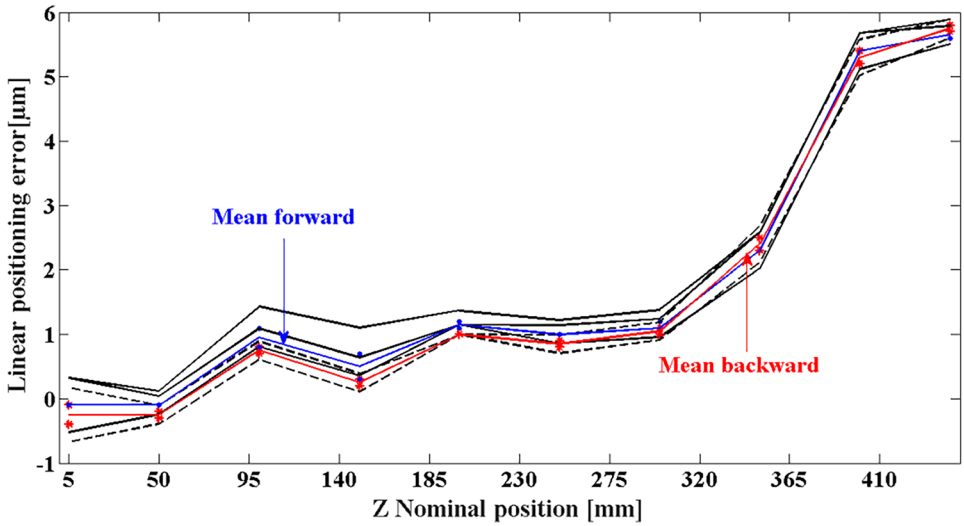

Fig. 8 Linear positioning errors, mean unidirectional and ± two unidirectional repeatability of the Z-axis of the Huron 8-five KX machine

According to Eqs. (18) and (19) and Figs. 10, 11, 12 and 13, the angular error motion around the *C*-axis (pitch) and the *A*-axis (roll) will affect the horizontal straightness error by the amounts of $E_{CX} \times t_{xbr}$, and $E_{AX} \times t_{zbr}$, respectively, while the angular error motion around the *B*-axis (yaw) and *A*-axis (roll) will affect the horizontal straightness error by the amounts of $E_{BX} \times t_{xbr} and E_{AX} \times t_{ybr}$, respectively. Furthermore, the larger the Bryan offset, the higher the correlation between the pitch, roll, yaw, and the straightness error. This means that the position of the straightness reflector on the machine table has a great effect on the measured straightness error.

4.3 Modeling of intra-axis errors

It is well known that indirect calibration of machine tool errors consists in the measurement of volumetric errors with an appropriate measuring instrument and the use of a linear parametric model establishing the relationships between the intra-axis errors, link errors, and the measured volumetric errors. This method usually requires using a function of representation for each intra-axis error and link errors with optimal numbers of coefficients or control points. Fewer coefficients (fewer control points) mean fewer unknowns and an improved numerical conditioning. Furthermore, the efficiency of parameter identification is primarily based on the analysis of the Jacobian matrix properties. The estimated coefficients (control points) are enhanced when the Jacobian has a low condition number. Previous studies [20] have shown experimentally that a 4-degree polynomial model is sufficient to represent the intra-axis error of a CNC machine tool. However, polynomials have been critiqued for their inflexibility and their very limited extrapolation. To account for these limitations, parametric models with 5 control points which is equivalent to a polynomial model with 5 coefficients (degree 4) is tested to represent the intra-axis errors. The present study shows that a Bézier model of degree 1 to 3 does not meet the required selection criteria, and provides a residual greater than the repeatability of the machine. However, a fourth degree Bézier model with 5 control points appears to be more robust, providing residuals identical to that of the polynomial model, and satisfying the selection criteria because

Table 3 Coefficients of correlation between the intra-axis errors of the *X*-axis of the Matsuura machine

X-axis	E_{XX}	E_{YX}	E_{ZX}	E_{BX}	E_{CX}
E_{XX}	1	−0.02	0.37	0.70	0.82
E_{YX}		1	0.50	0.18	0.06
E_{ZX}			1	0.03	0.30
E_{BX}				1	0.37
E_{CX}					1

Table 4 Coefficients of correlation between the intra-axis errors of the *Y*-axis of the Matsuura machine

Y-axis	E_{XY}	E_{YY}	E_{ZY}	E_{AY}	E_{CY}
E_{XY}	1	0.30	0.26	−0.19	−0.06
E_{YY}		1	0.24	−0.83	0.84
E_{ZY}			1	−0.59	0.67
E_{AY}				1	−0.76
E_{CY}					1

Table 5 Coefficients of correlation between the intra-axis errors of the *Z*-axis of the Matsuura machine

Z-axis	E_{XZ}	E_{YZ}	E_{ZZ}	E_{AZ}	E_{BZ}
E_{XZ}	1	0.51	−0.68	0.96	−0.75
E_{YZ}		1	−0.17	0.66	−0.40
E_{ZZ}			1	−0.96	0.81
E_{AZ}				1	−0.74
E_{BZ}					1

the residual is within the repeatability range of the tested axis (Figs. 14, 15 and 16). On the other hand, the results also show that a second degree B-spline model with 5 control points meets the selection criterion well (Figs. 14, 15 and 16). The offset between the two curves (backward and forward) in Figs. 14, 15 and 16 indicates the influence of the backlash error.

Equations (18) and (20) show the selected Bézier and B-spline models, respectively.

For the Bézier model:

$$P(u) = \sum_{i=0}^{n=4} B_{i,4}(u).P_i \tag{20}$$

$$P(u) = B_{0,4}(u).P_0 + B_{1,4}(u).P_1 + B_{2,4}(u).P_2 + B_{3,4}(u).P_3 + B_{4,4}(u).P_4 \tag{21}$$

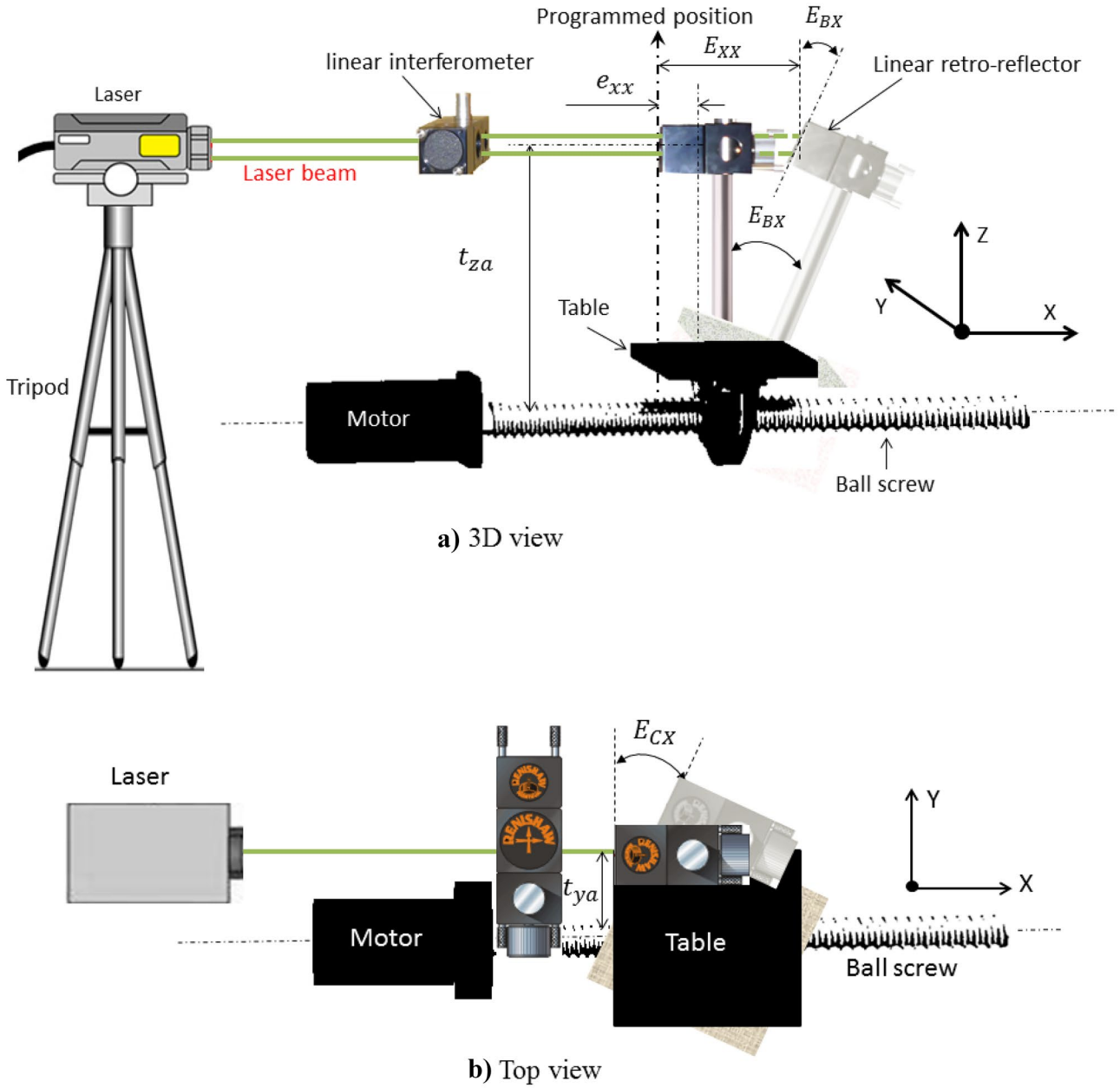

Fig. 9 Linear positioning error measurement with Abbe error

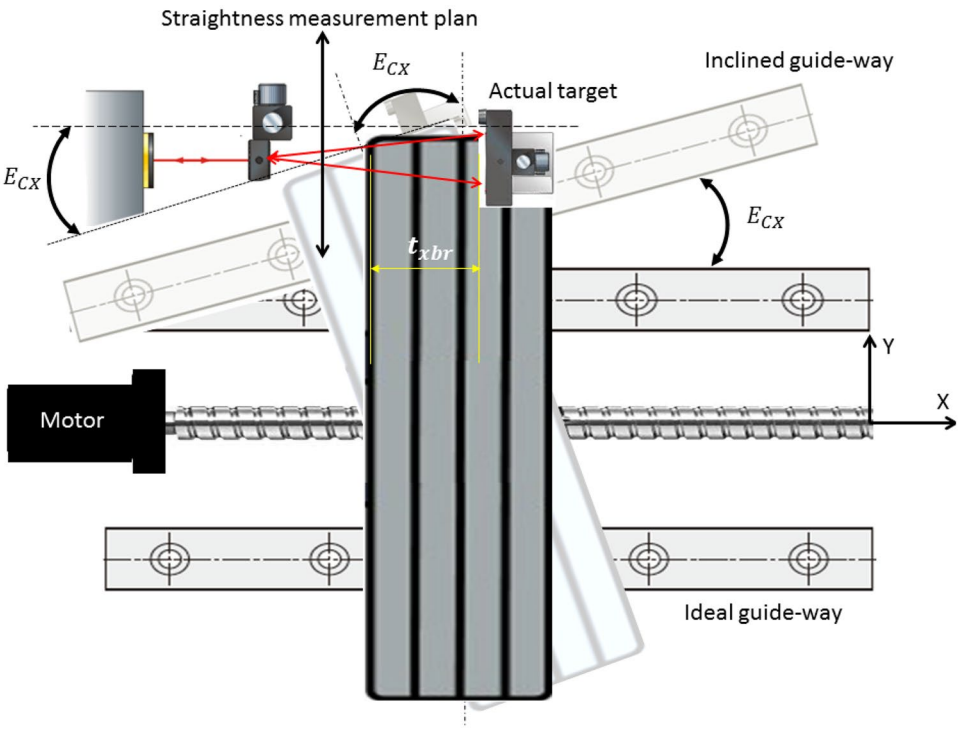

Fig. 10 Angular error motion around C-axis (E_{CX}) due to horizontally non-parallel guideways

For the B-spline model:

$$P(u) = \sum_{i=0}^{n=4} N_{i,3}(u).P_i \tag{22}$$

$$P(u) = N_{0,3}(u).P_0 + N_{1,3}(u).P_1 + N_{2,3}(u).P_2 + N_{3,3}(u).P_3 + N_{4,3}(u).P_4 \tag{23}$$

The basis functions $B_{i,4}(u)$ and $N_{i,3}(u)$ and $i = 0, 1, \ldots 4$ are calculated based on Eqs. (1) and (5), respectively.

After a proper optimization process, a spline and Bezier curves are fully defined if the control points P_i and the basis functions $B_{i,n}$ and $N_{i,n}$ are well defined. In this study, a uniform and fixed knots vector is used. By fixing the knot vector, only the control points have to be optimized. This allows as reducing the B-spline fitting problem to a linear least squares problem.

The Bézier and B-spline control points of Eqs. (18) and (20) can be estimated using the least square method. Accordingly, the control points ($P_i, i = 0, 1 \ldots 4$) of each model of the intra-axis error are estimated and presented in Tables 6, 7, 8, 9, 10 and 11 in the appendix.

As explained earlier, four statistical indices were used to select the most accurate model. First, the selection

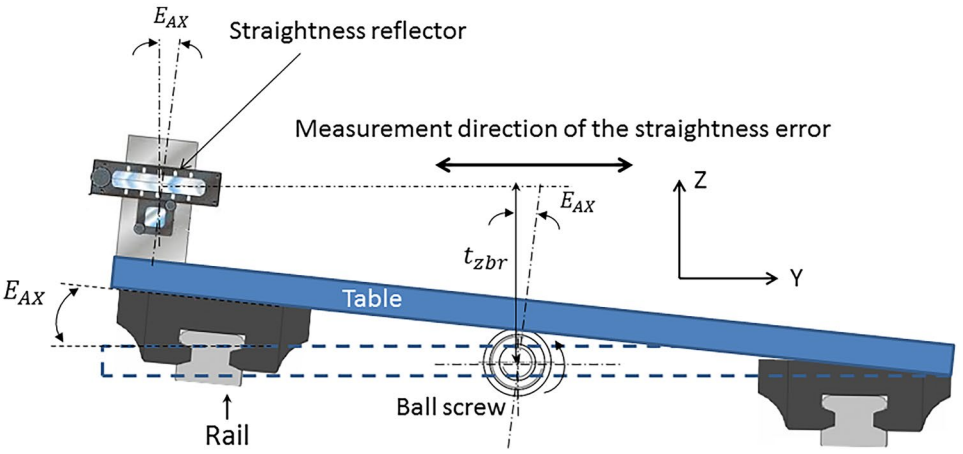

Fig. 11 Angular error motion around A-axis (roll; E_{AX}) and its effect on the horizontal straightness error

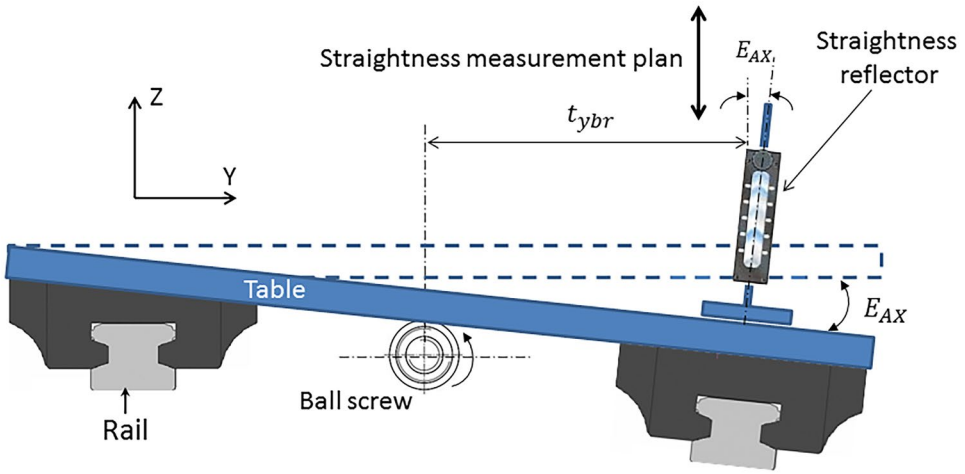

Fig. 12 Angular error motion around *A*-axis (roll) and its effect on the vertical straightness error

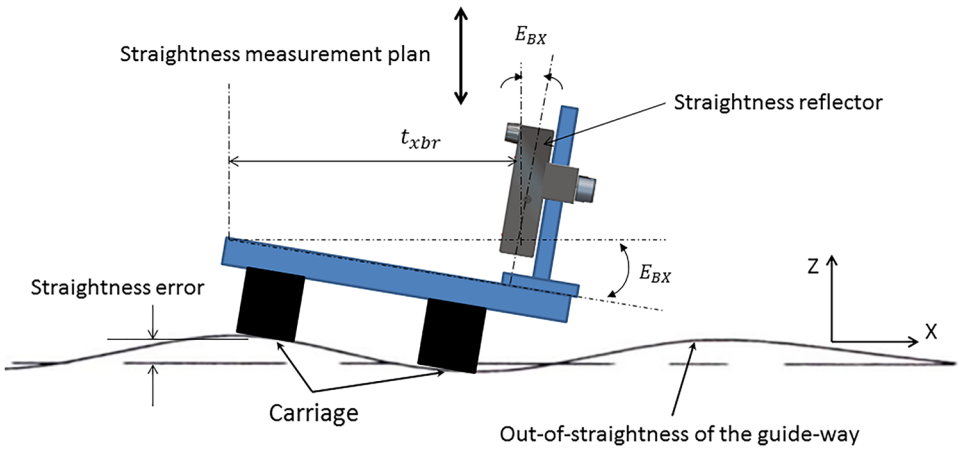

Fig. 13 Angular error motion around *B*-axis (yaw) and its effect on the vertical straightness error

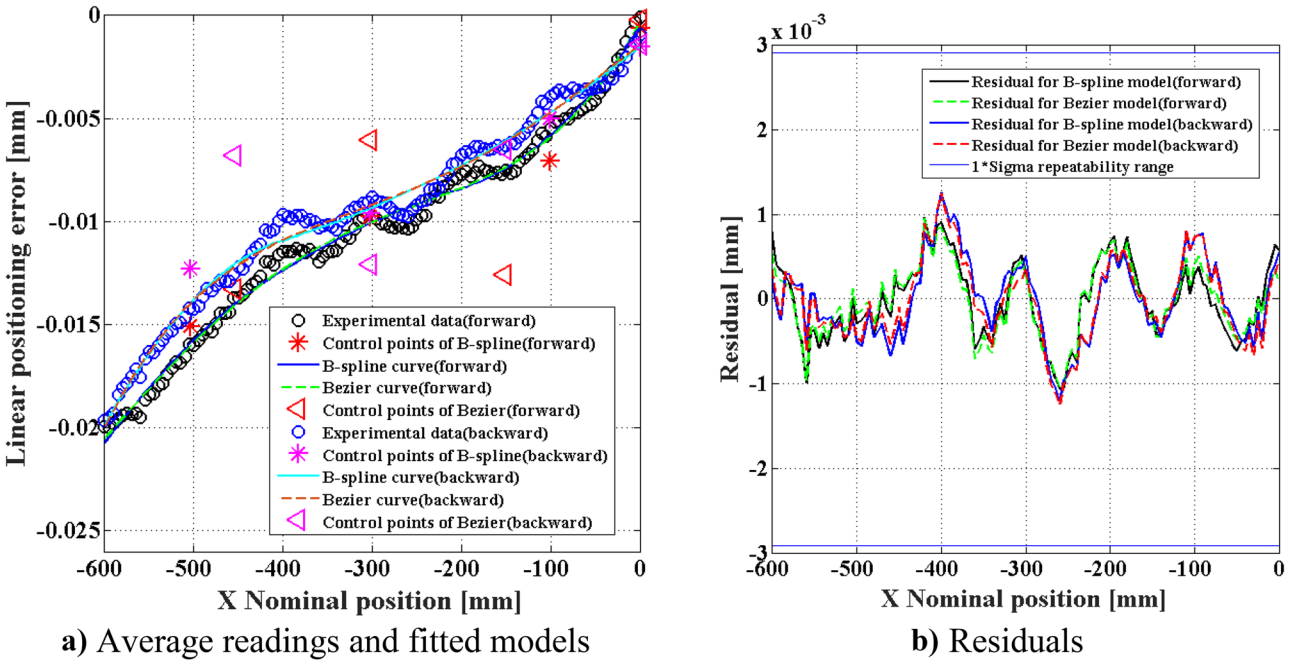

a) Average readings and fitted models **b)** Residuals

Fig. 14 Linear positioning error of the *X*-axis of the Mitsui Seiki HU40 machine. **a** Average readings and fitted models. **b** Residuals

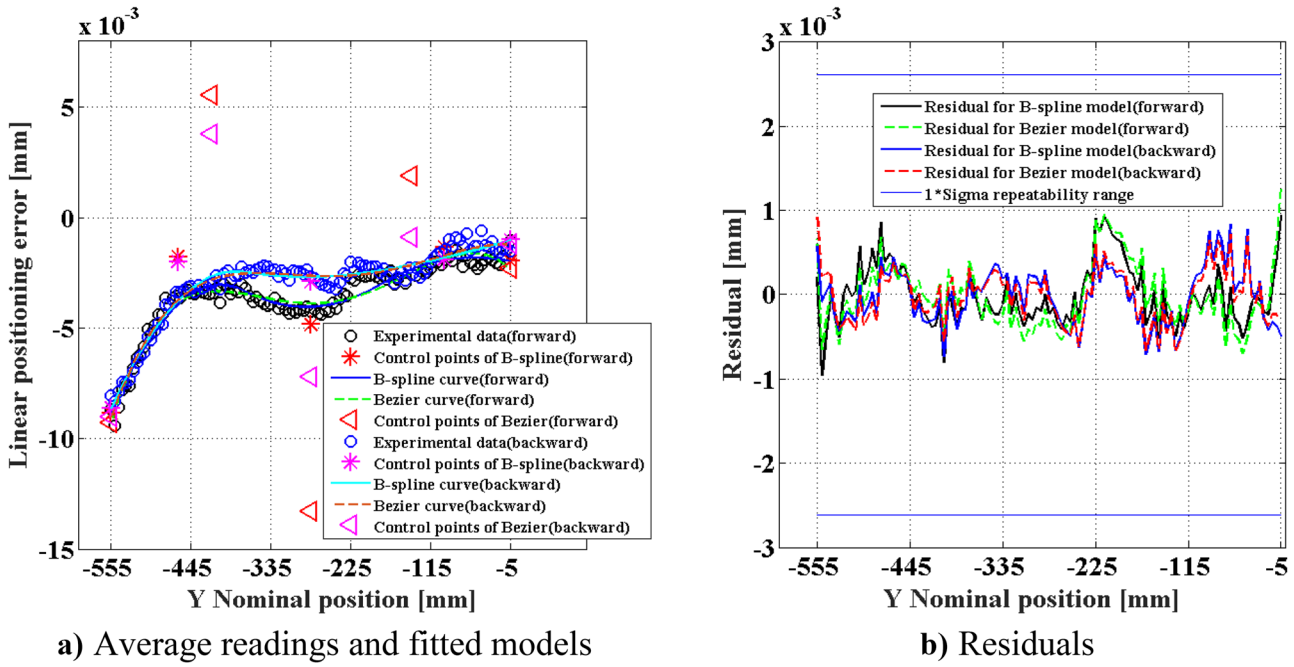

a) Average readings and fitted models **b)** Residuals

Fig. 15 Linear positioning error of the *Y*-axis of the Mitsui Seiki HU40 machine. **a** Average readings and fitted models. **b** Residuals

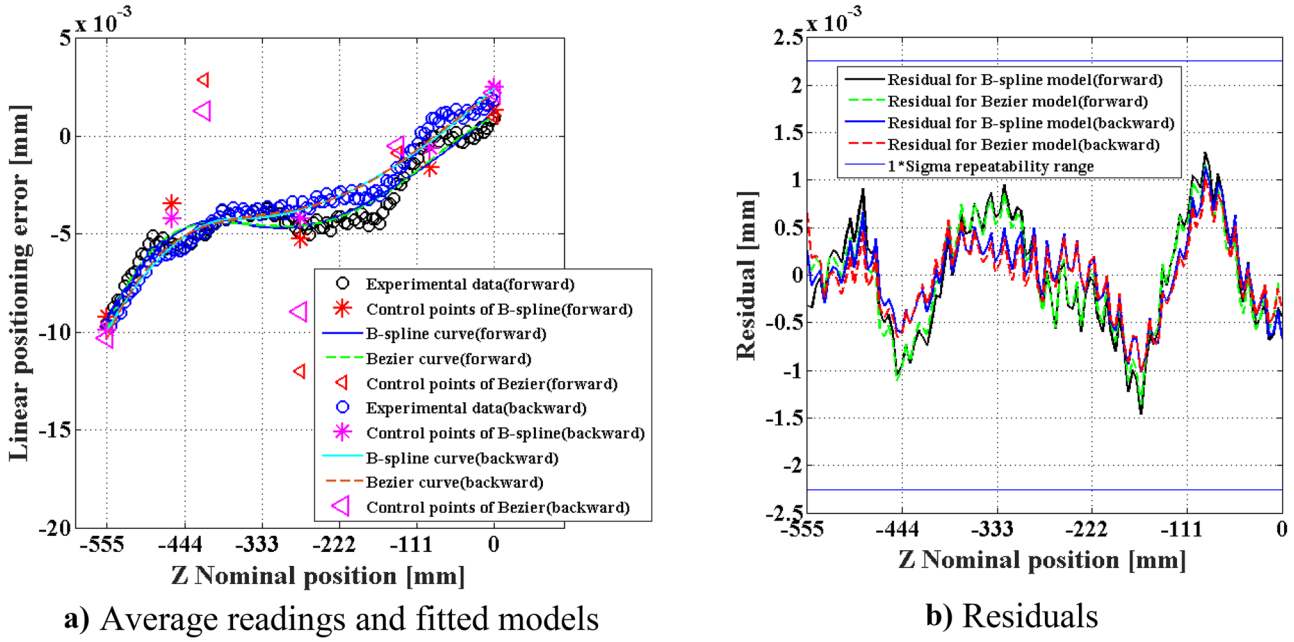

a) Average readings and fitted models **b)** Residuals

Fig. 16 Linear positioning error of the *Z*-axis of the Mitsui Seiki HU40 machine. **a** Average readings and fitted models. **b** Residuals

Table 6 Comparison of the statistical indices of the three models for the linear positioning errors of the three tested machines

IAES	Statistical indices	Matsuura						Mitsui Seiki						Huron					
		Forward			Backward			Forward			Backward			Forward			Backward		
		Poly	Bz	Bs	Poly	Bz	Bs	Poly	Bz	Bs	Poly	Bz	Bs	Poly	Bz	Bs	Poly	Bz	Bs
E_{XX}	R^2	0.98	0.98	0.99	0.98	0.98	0.98	0.99	0.99	0.99	0.99	0.99	0.99	0.99	0.99	0.99	0.99	0.99	0.99
	RMSE (μm)	0.17	0.17	0.15	0.19	0.19	0.18	0.43	0.43	0.47	0.49	0.49	0.49	0.70	0.70	0.70	0.70	0.70	0.69
	MAE (μm)	0.13	0.13	0.12	0.16	0.16	0.15	0.36	0.36	0.39	0.40	0.40	0.40	0.62	0.62	0.62	0.61	0.61	0.60
	MAPE %	16.6	16.6	13.8	26.7	26.7	25.3	8.3	8.3	10.0	6.1	6.1	6.1	50.2	50.2	54.3	12.2	12.2	12.7
E_{YY}	R^2	0.99	0.99	0.99	0.99	0.99	0.99	0.94	0.94	0.94	0.96	0.96	0.96	0.93	0.93	0.94	0.94	0.94	0.94
	RMSE (μm)	0.80	0.80	0.80	0.48	0.48	0.43	0.39	0.39	0.37	0.32	0.32	0.34	1.20	1.20	1.20	1.17	1.17	1.16
	MAE (μm)	0.70	0.70	0.70	0.40	0.40	0.38	0.31	0.31	0.29	0.26	0.26	0.28	1.11	1.11	1.11	1.1	1.1	1.1
	MAPE %	3.58	3.58	3.60	12.33	12.33	10.88	10.95	10.95	9.76	12.30	12.30	13.92	66.61	66.61	66.75	127.2	127.2	126.0
E_{ZZ}	R^2	0.99	0.99	0.99	0.99	0.99	0.99	0.95	0.95	0.93	0.98	0.98	0.98	0.93	0.93	0.93	0.95	0.95	0.95
	RMSE (μm)	0.13	0.13	0.13	0.10	0.10	0.10	0.54	0.54	0.60	0.40	0.40	0.43	0.51	0.51	0.52	0.47	0.47	0.48
	MAE (μm)	0.11	0.11	0.11	0.08	0.08	0.08	0.45	0.45	0.51	0.32	0.32	0.35	0.43	0.43	0.43	0.40	0.40	0.40
	MAPE %	12.06	12.06	11.97	0.60	0.60	0.60	171.87	171.87	193.83	21.47	21.47	24.74	102.9	102.9	83.92	55.90	55.90	50.18

approach was applied on the results of the Matsuura machine. In order to assess the generality of the selected models, additional tests were carried out on two other types of machine tools with different controllers and guidance technologies. Table 12 shows the linear positioning errors of the three tested machines. By taking the polynomial model as reference, it can be seen from Table 12 that both models are adequate and have a very high R-squared. Moreover, the results show that the four statistical indices for the polynomial and Bézier models are identical. Furthermore, the four statistical indices of the Bézier and B-spline models are almost the same, with the B-spline model having a small advantage in terms of prediction accuracy.

The results of the pitch (Figs. 17 and 18) and yaw (Figs. 19 and 20) errors presented in Table 13 show that both models remain adequate in most cases. It can also be observed from Figs. 17, 18, 19 and 20 that the backlash of the yaw error is greater than that of the pitch error.

The approach is also assessed on new results obtained from the Huron 8-five KX machine with the Renishaw laser interferometer measurement system. Figures 21, 22 and 23 show the results of the linear positioning errors of the three axes of the Huron machine. They show that both models provide high fit quality.

The horizontal and vertical straightness errors of the Huron machine are presented in Figs. 24 and 25. It can be seen from these figures that the magnitude of the straightness errors is small as compared to the linear positioning errors. Furthermore, the lateral backlash is small, and in some cases, negligible. On the other hand, a closer look at these figures reveals that the capability of the models to represent the straightness errors decreases thanks to the small magnitude of the straightness errors, which in some cases is close to the repeatability of the reading.

Most residuals presented above show a periodic behavior not captured by the models. This periodic behavior is often of relatively high frequency, which is difficult to capture with Bézier or B-spline models. This kind of behavior requires complimentary models with periodic functions. However, the tested models represent well the low frequency oscillation resulting from the slow variation of the geometric error along the measured axis.

Overall, and from a machine tool metrology perspective, the B-spline and Bézier models show very competitive characteristics in all the comparisons. Furthermore, the flexibility and the differentiability [51, 52] of these models in turn contribute to their status as alternatives to the polynomial models for the modeling of intra-axis errors, and hence, they can be integrated into the geometric error Jacobian matrix during the indirect calibration process of a CNC machine tool.

Table 7 Comparison of the statistical indices of the three models for the angular errors of the Matsuura and Mitsui Seiki machines

IAES	Statistical indices	Matsuura						Mitsui Seiki					
		Forward			Backward			Forward			Backward		
		Poly	Bz	Bs	Poly	Bz	Bs	Poly	Bz	Bs	Poly	Bz	Bs
E_{BX}	R^2	0.98	0.98	0.98	0.97	0.97	0.97	0.83	0.83	0.82	0.75	0.75	0.75
	RMSE (arcsec)	0.13	0.13	0.14	0.14	0.14	0.14	0.19	0.19	0.19	0.22	0.22	0.22
	MAE (arcsec)	0.10	0.10	0.10	0.10	0.10	0.10	0.15	0.15	0.15	0.18	0.18	0.18
	MAPE %	7.85	7.85	8.67	4.60	4.60	4.64	8.8	8.8	9.8	10.2	10.2	11.2
E_{CX}	R^2	0.93	0.93	0.93	0.93	0.93	0.93	0.80	0.80	0.79	0.91	0.91	0.91
	RMSE (arcsec)	0.13	0.13	0.13	0.12	0.12	0.12	0.19	0.19	0.20	0.15	0.15	0.15
	MAE (arcsec)	0.11	0.11	0.11	0.10	0.10	0.10	0.15	0.15	0.15	0.11	0.11	0.11
	MAPE %	7.56	7.56	7.67	6.09	6.09	6.03	9.5	9.5	8.5	11.2	11.2	10.9
E_{AY}	R^2	0.75	0.75	0.76	0.72	0.72	0.72	0.93	0.93	0.93	0.96	0.96	0.96
	RMSE (arcsec)	0.13	0.13	0.13	0.15	0.15	0.15	1.97	1.97	1.97	2.00	2.00	2.00
	MAE (arcsec)	0.12	0.12	0.12	0.11	0.11	0.11	1.52	1.52	1.52	1.71	1.71	1.71
	MAPE %	13.2	13.2	12.1	15.2	15.2	14.3	7.8	7.8	6.7	7.6	7.6	5.9
E_{CY}	R^2	0.95	0.95	0.94	0.95	0.95	0.95	0.76	0.76	0.78	0.75	0.75	0.78
	RMSE (arcsec)	0.09	0.09	0.09	0.08	0.08	0.08	0.78	0.78	0.77	0.68	0.68	0.68
	MAE (arcsec)	0.07	0.07	0.08	0.06	0.06	0.06	0.67	0.67	0.66	0.59	0.59	0.59
	MAPE %	8.2	8.2	9.1	7.77	7.77	7.2	12.2	12.2	11.3	12.8	12.8	14.1
E_{AZ}	R^2	0.95	0.95	0.95	0.94	0.94	0.94	0.79	0.79	0.80	0.74	0.74	0.72
	RMSE (arcsec)	0.12	0.12	0.11	0.15	0.15	0.15	0.20	0.20	0.19	0.1751	0.1751	0.17
	MAE (arcsec)	0.09	0.09	0.09	0.12	0.12	0.12	0.16	0.16	0.16	0.14	0.14	0.14
	MAPE %	15.3	15.3	14.2	13.86	13.86	11.05	15.3	15.3	15.1	16.44	16.44	15.44
E_{BZ}	R^2	0.83	0.83	0.84	0.87	0.87	0.87	0.92	0.92	0.92	0.94	0.94	0.94
	RMSE (arcsec)	0.09	0.09	0.09	0.13	0.13	0.13	0.14	0.14	0.14	0.13	0.13	0.13
	MAE (arcsec)	0.07	0.07	0.07	0.11	0.11	0.11	0.11	0.11	0.11	0.11	0.11	0.11
	MAPE %	11.73	11.73	13.12	14.37	14.37	12.92	13.5	13.5	10.1	9.32	9.32	9.42

5 Conclusion

A correlation assessment and modeling of the intra-axis errors are fundamental to improving the performance of the CNC machine tool. From experimental observations, the correlation between intra-axis errors is evaluated in this paper. Furthermore, this work developed and evaluated two prediction models (Bézier and B-spline). Based on the experimental data, the control points of each model were estimated. To choose the degree of the model and the number of the control points in a rigorous way, statistical criteria were applied.

Based on the experiments and analysis conducted, the following observations were made:

- The results show that there is no correlation between the linear positioning error E_{XX} and the horizontal straightness error E_{YX}. However, a strong correlation was observed between the linear positioning error and the pitch and yaw error. This observation was confirmed for the three tested machines.
- No correlation was observed between the horizontal straightness error E_{YX} and the yaw error E_{BX}. Similarly, no correlation was seen between the straightness error E_{ZX} and E_{CX}.
- The analysis of the residuals shows that a Bézier model of degree four and a B-spline model of degree two, both with five control points, satisfy the selection criteria.
- In terms of meeting the performance criteria, the two suggested models are adequate, but the B-spline model performs slightly better in terms of prediction accuracy.
- To generalize our approach, additional tests were carried out on two other types of machines with different controllers and guidance technologies. The results show that the two proposed models remained valid.
- This study shows that the parametric models can be used successfully as alternatives to the polynomial models for the modeling of intra-axis errors of a CNC machine tool.

Appendix

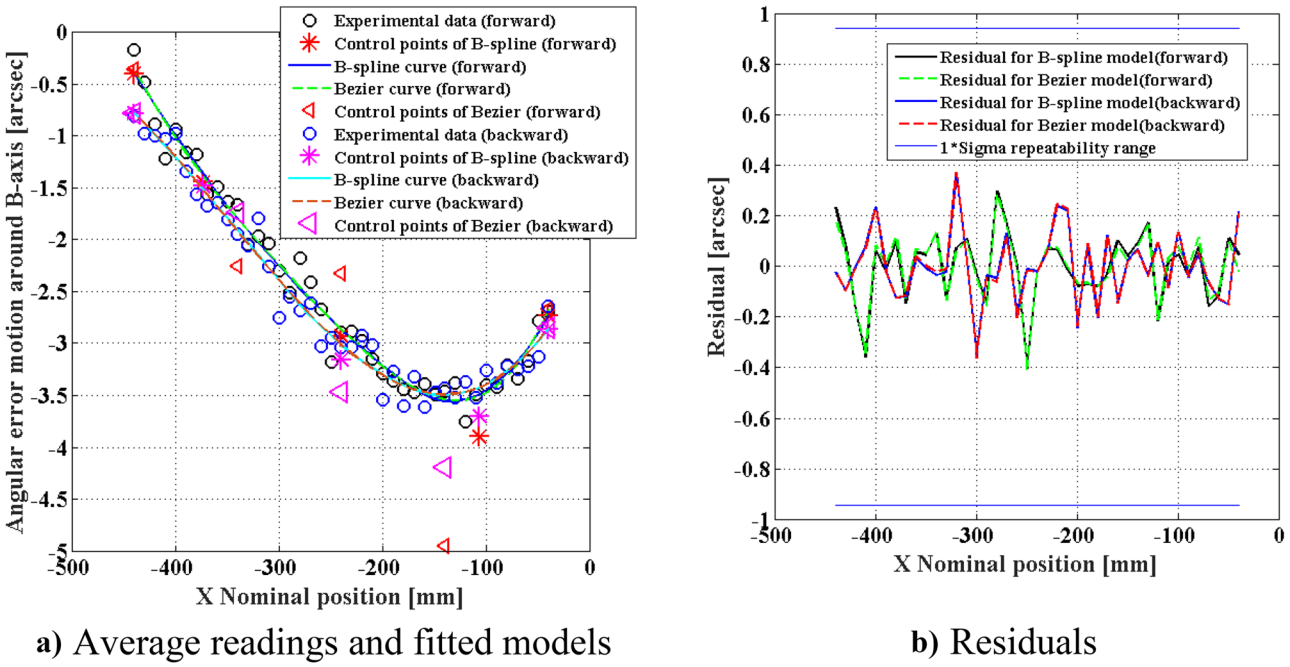

Fig. 17 Angular error motion around *B*-axis of the *X*-axis (E_{BX}) of the Matsuura machine. **a** Average readings and fitted models. **b** Residuals

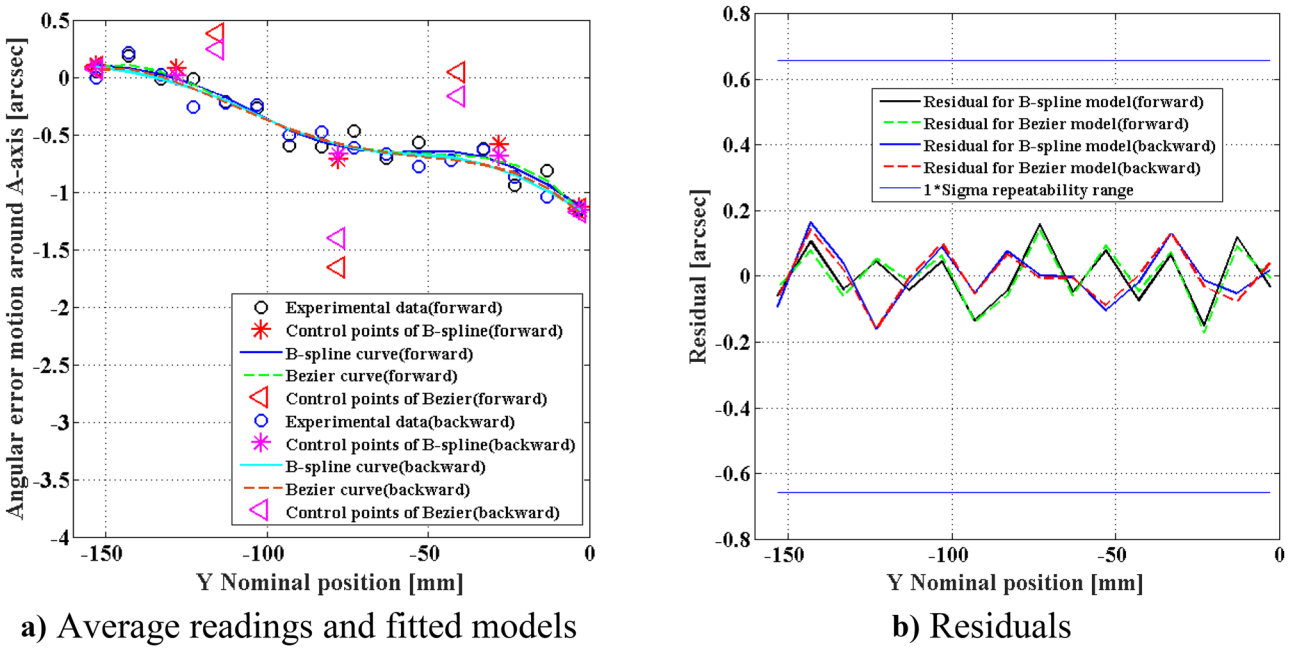

Fig. 18 Angular error motion around *A*-axis of the *Y*-axis (E_{AY}) of the Matsuura machine. **a** Average readings and fitted models. **b** Residuals

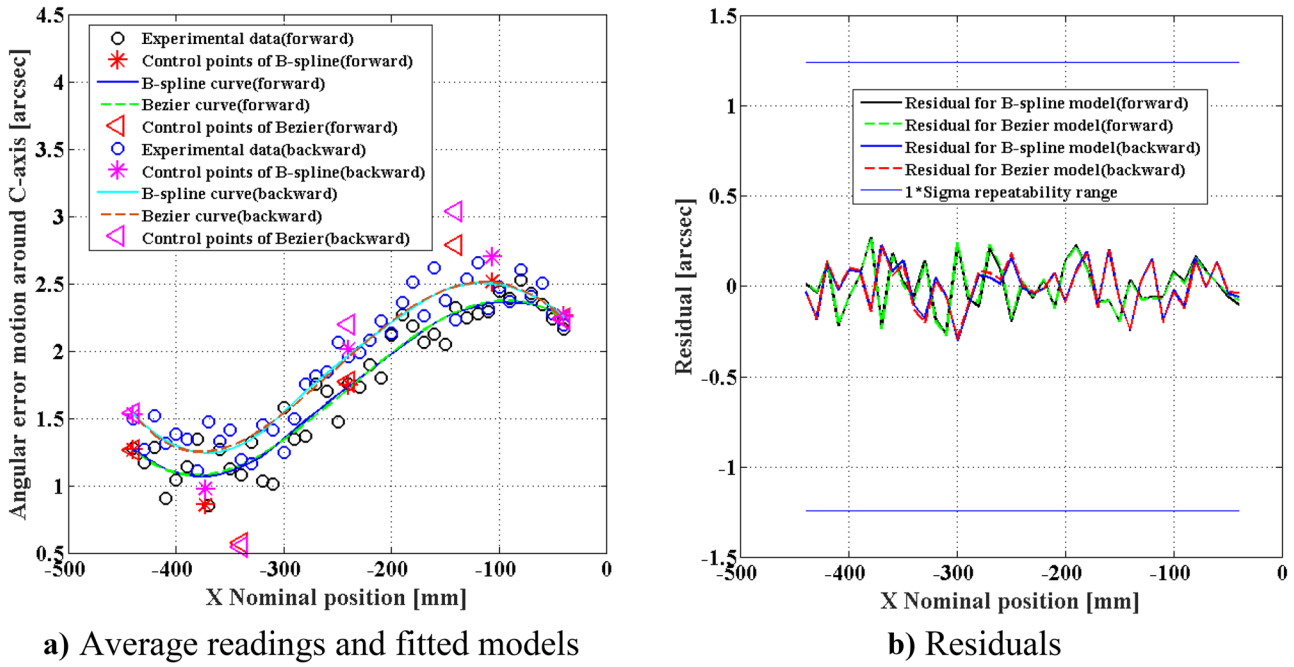

Fig. 19 Angular error motion around *C*-axis of the *X*-axis (E_{CX}) of the Matsuura machine. **a** Average readings and fitted models. **b** Residuals

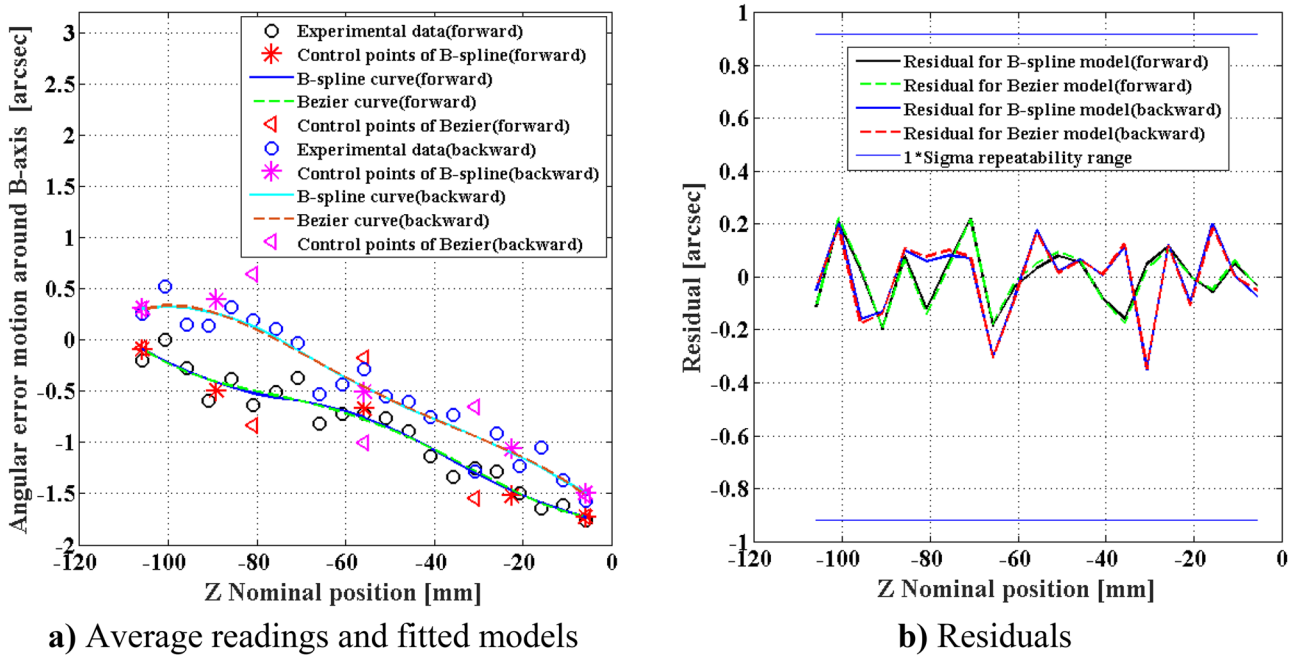

Fig. 20 Angular error motion around *B*-axis of the *Z*-axis (E_{BZ}) of the Matsuura machine. **a** Average readings and fitted models. **b** Residuals

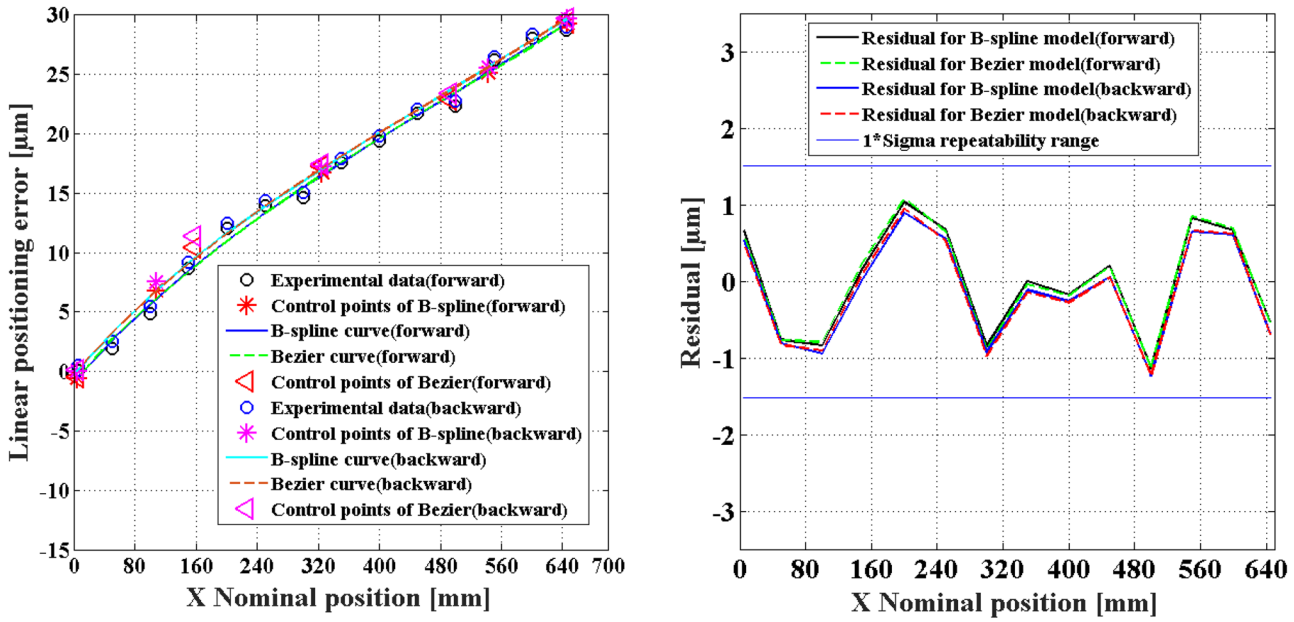

a) Average readings and fitted models **b)** Residuals

Fig. 21 Linear positioning error of the X-axis (E_{XX}) of the Huron 8-five KX machine. **a** Average readings and fitted models. **b** Residuals

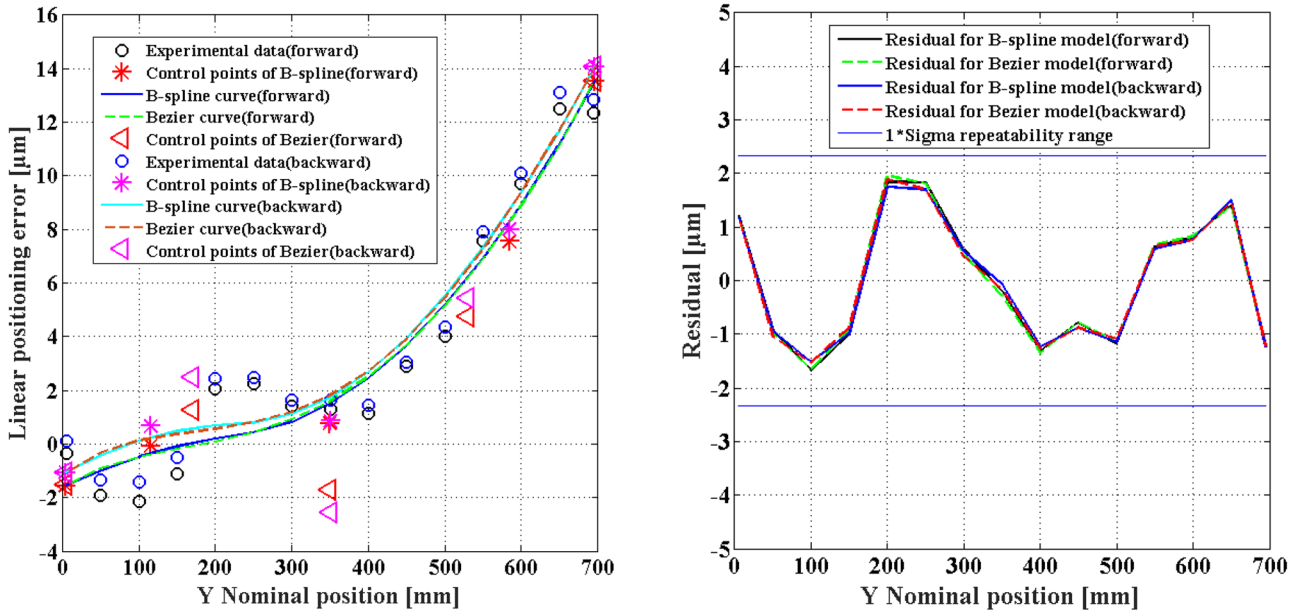

a) Average readings and fitted models **b)** Residuals

Fig. 22 Linear positioning error of the Y-axis (E_{YY}) of the Huron 8-five KX machine. **a** Average readings and fitted models. **b** Residuals

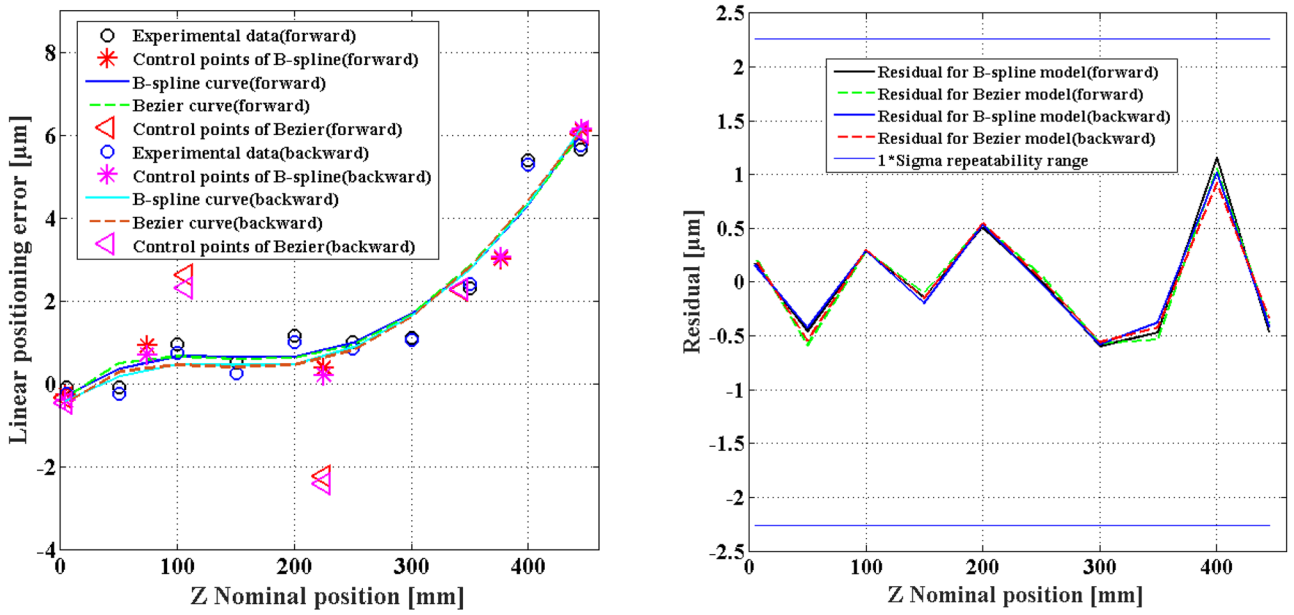

a) Average readings and fitted models **b)** Residuals

Fig. 23 Linear positioning error of the *Z*-axis (E_{ZZ}) of the Huron 8-five KX machine. **a** Average readings and fitted models. **b** Residuals

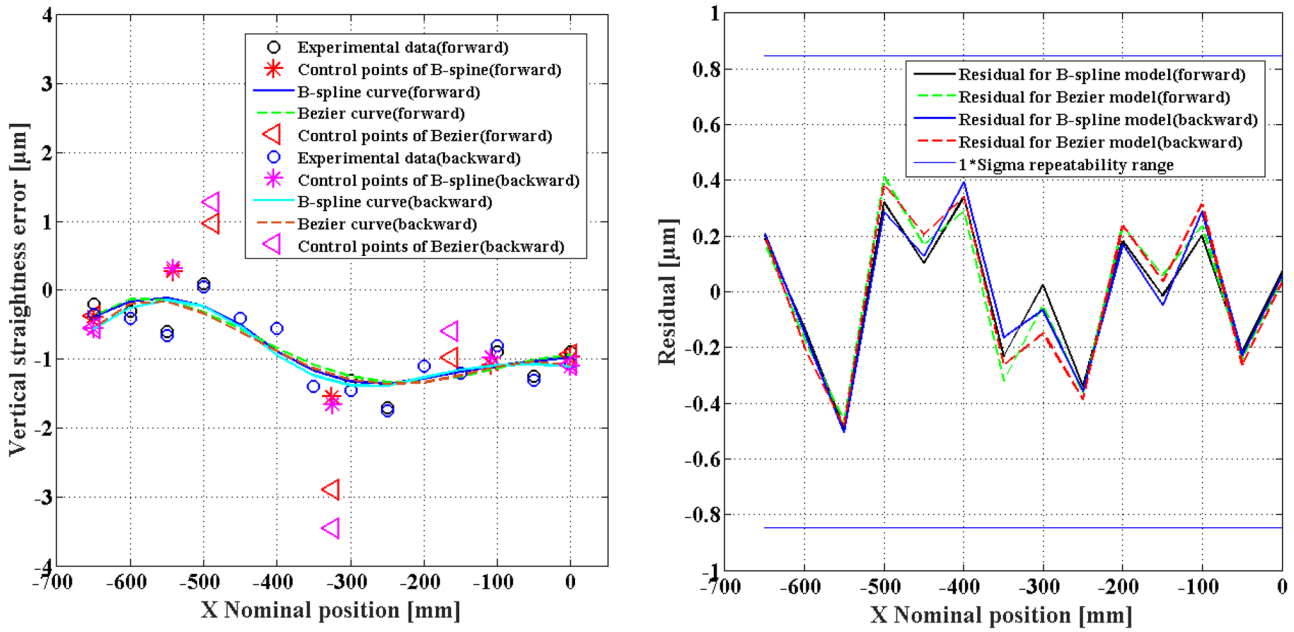

a) Average readings and fitted models **b)** Residuals

Fig. 24 Vertical straightness error of the *X*-axis (E_{ZX}) of the Huron 8-five KX machine. **a** Average readings and fitted models. **b** Residuals

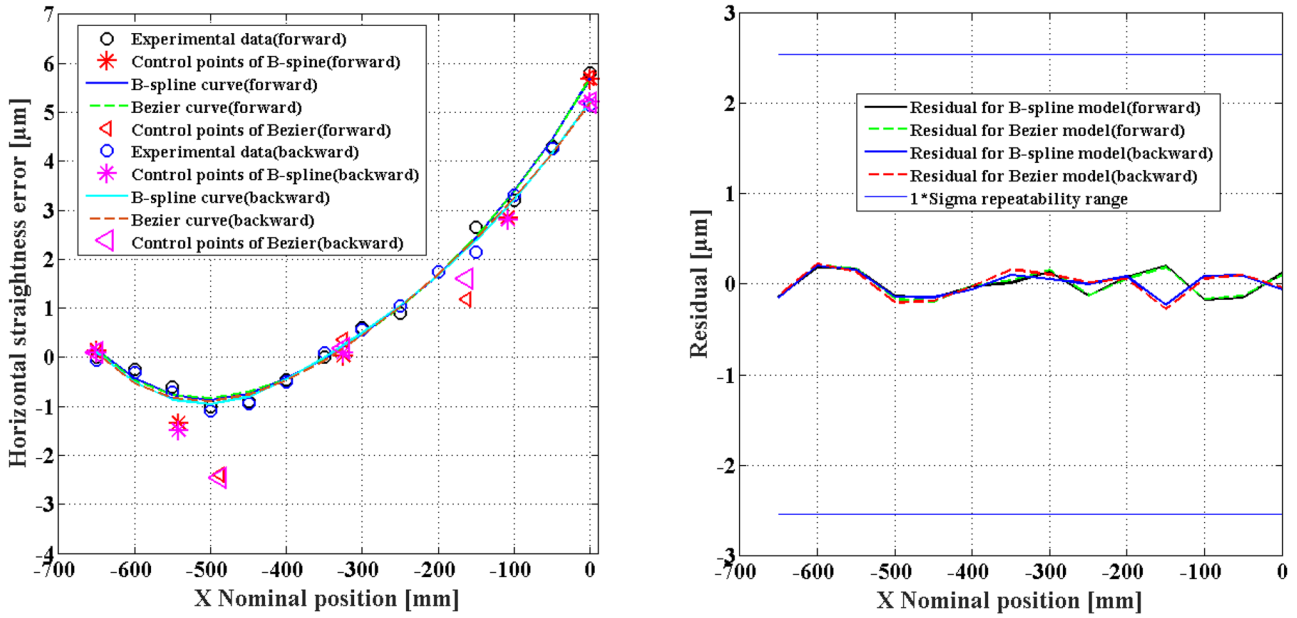

a) Average readings and fitted models **b)** Residuals

Fig. 25 Horizontal straightness error of the *X*-axis (E_{YX}) of the Huron 8-five KX machine. **a** Average readings and fitted models. **b** Residuals

Table 8 Estimated control points of the Bezier (Bz) and B-spline (Bs) models for the intra-axis errors (IAEs) in the forward direction of the *X*-axis of the Matsuura machine tool

Axis	IAEs		Control points				
			P0	P1	P2	P3	P4
X	E_{XX}	Bz	(−440; 0.0009)	(−340; −0.0040)	(−240; −0.0033)	(−140; −0.0065)	(−40; 0.0019)
		Bs	(−440; 0.0008)	(−373.3333; −0.0021)	(−240; −0.0040)	(−106.6667; −0.0032)	(−40; 0.0019)
	E_{YX}	Bz	(−440; 0.0004)	(−340; −0.0012)	(−240; −0.0011)	(−140; 0.0016)	(−40; −0.0010)
		Bs	(−440; 0.0004)	(−373.3333; −0.0007)	(−240; −0.0004)	(−106.6667; 0.0004)	(−40; −0.0009)
	E_{ZX}	Bz	(−440; 0.0018)	(−340; 0.0018)	(−240; 0.0008)	(−140; 0.0011)	(−40; −0.0001)
		Bs	(−440; 0.0018)	(−373.3333; −0.0011)	(−240; −0.0000)	(−106.6667; 0.0007)	(−40; −0.0001)
	E_{BX}	Bz	(−440; 1.2661)	(−340; 0.5727)	(−240; 1.7685)	(−140; 2.7887)	(−40; 2.2401)
		Bs	(−440; 1.2671)	(−373.3333; 0.8572)	(−240; 1.7518)	(−106.6667; 2.5186)	(−40; 2.2672)
	E_{CX}	Bz	(−440; −0.3541)	(−340; −2.2577)	(−240; −2.3297)	(−140; −4.9578)	(−40; −2.6731)
		Bs	(−440; −0.3999)	(−373.3333; −1.4440)	(−240; −2.9325)	(−106.6667; −3.8968)	(−40; −2.7370)

Table 9 Estimated control points of the Bezier (Bz) and B-spline (Bs) models for the intra-axis errors in the backward direction of the *X*-axis of the Matsuura machine tool

Axis	IAEs		Control points				
			P0	P1	P2	P3	P4
X	E_{XX}	Bz	(−440; 0.0002)	(−340; −0.0040)	(−240; −0.0040)	(−140; −0.0062)	(−40; 0.0016)
		Bs	(−440; 0.0002)	(−373.3333; −0.0024)	(−240; −0.0043)	(−106.6667; −0.0033)	(−40; 0.0015)
	E_{YX}	Bz	(−440; 0.0008)	(−340; −0.0013)	(−240; 0)	(−140; 0.0010)	(−40; −0.0002)
		Bs	(−440; 0.0008)	(−373.3333; −0.0005)	(−240; 0.0000)	(−106.6667; 0.0005)	(−40; −0.0002)
	E_{ZX}	Bz	(−440; 0.0010)	(−340; −0.0038)	(−240; 0.0008)	(−140; 0.0004)	(−40; −0.0008)
		Bs	(−440; 0.0010)	(−373.3333; −0.0017)	(−240; −0.0004)	(−106.6667; 0.0001)	(−40; −0.0008)
	E_{BX}	Bz	(−440; 1.5339)	(−340; 0.5452)	(−240; 2.1945)	(−140; 3.0397)	(−40; 2.2344)
		Bs	(−440; 1.5291)	(−373.3333; 0.9752)	(−240; 2.0141)	(−106.6667; 2.7032)	(−40; 2.2561)
	E_{CX}	Bz	(−440; −0.7852)	(−340; −1.7416)	(−240; −3.4682)	(−140; −4.1992)	(−40; −2.8521)
		Bs	(−440; −0.7792)	(−373.3333; −1.4835)	(−240; −3.1575)	(−106.6667; −3.7022)	(−40; −2.8602)

Table 10 Estimated control points of the Bezier (Bz) and B-spline (Bs) models for the intra-axis errors in the forward direction of the Y-axis of the Matsuura machine tool

Axis	IAEs		Control points				
			P0	P1	P2	P3	P4
Y	E_{XY}	Bz	(−153; 0.0030)	(−115.5; 0.0032)	(−78; 0.0022)	(−40.5; 0.0030)	(−3; −0.0003)
		Bs	(−153; 0.0030)	(−128; 0.0030)	(−78; 0.0026)	(−28;0.0016)	(−3; −0.0003)
	E_{YY}	Bz	(−153; −0.0017)	(−115.5; 0.0034)	(−78; −0.0015)	(−40.5; 0.0017)	(−3; −0.0009)
		Bs	(−153; −0.0016)	(−128; 0.0011)	(−78; 0.0004)	(−28; 0.0004)	(−3; −0.0009)
	E_{ZY}	Bz	(−153; 0.0003)	(−115.5; −0.0018)	(−78; 0.0021)	(−40.5; 0.0001)	(−3; −0.0004)
		Bs	(−153; 0.0003)	(−128; −0.0007)	(−78; 0.0006)	(−28; 0.0001)	(−3; −0.0005)
	E_{AY}	Bz	(−153; −0.1087)	(−115.5; −0.4848)	(−78; 0.0558)	(−40.5; 0.0922)	(−3; 0.5173)
		Bs	(−153; −0.1101)	(−128; −0.3112)	(−78; −0.0644)	(−28; 0.2790)	(−3; 0.5034)
	E_{CY}	Bz	(−153; 0.0928)	(−115.5; 0.3883)	(−78; −1.6571)	(−40.5; 0.0505)	(−3; −1.1476)
		Bs	(−153; 0.1139)	(−128; 0.0885)	(−78; −0.7114)	(−28; −0.5750)	(−3; −1.1217)

Table 11 Estimated control points of the Bezier (Bz) and B-spline (Bs) models for the intra-axis errors in the backward direction of the *Y*-axis of the Matsuura machine tool

Axis	IAEs		Control points				
			P0	P1	P2	P3	P4
Y	E_{XY}	Bz	(−153; −0.0001)	(−115.5; −0.0008)	(−78; 0.0006)	(−40.5; −0.0010)	(−3; −0.0032)
		Bs	(−153; −0.0001)	(−128; −0.0004)	(−78; −0.0002)	(−28; −0.0017)	(−3; −0.0032)
	E_{YY}	Bz	(−153; −0.0020)	(−115.5; 0.0040)	(−78; −0.0022)	(−40.5; 0.0023)	(−3; −0.0012)
		Bs	(−153; −0.0020)	(−128; 0.0013)	(−78; 0.0003)	(−28; 0.0005)	(−3; −0.0012)
	E_{ZY}	Bz	(−153; 0.0000)	(−115.5; −0.0012)	(−78; 0.0008)	(−40.5; 0.0007)	(−3; −0.0004)
		Bs	(−153; 0.0002)	(−128; −0.0006)	(−78; 0.0003)	(−28; 0.0002)	(−3; −0.0004)
	E_{AY}	Bz	(−153; −0.4944)	(−115.5; 0.5543)	(−78; −0.7596)	(−40.5; 0.7521)	(−3; 0.2967)
		Bs	(−153; −0.4831)	(−128; 0.0485)	(−78; −0.0748)	(−28; 0.4602)	(−3; 0.3059)
	E_{CY}	Bz	(−153; 0.0724)	(−115.5; 0.2508)	(−78; −1.4037)	(−40.5; −0.1597)	(−3; −1.1734)
		Bs	(−153; 0.0976)	(−128; 0.0196)	(−78; −0.6647)	(−28; −0.6775)	(−3; −1.1535)

Table 12 Estimated control points of the Bezier (Bz) and B-spline (Bs) models for the intra-axis errors in the forward direction of the Z-axis of the Matsuura machine tool

Axis	IAEs		Control points				
			P0	P1	P2	P3	P4
Z	E_{XZ}	Bz	(−105.8; −0.0003)	(−80.8; −0.0008)	(−55.8; −0.0011)	(−30.8; −0.0038)	(−5.8; −0.0039)
		Bs	(−105.8; −0.0004)	(−89.1333; −0.0006)	(−55.8; −0.0017)	(−22.4667; −0.0036)	(−5.8; −0.0039)
	E_{YZ}	Bz	(−105.8; 0.0004)	(−80.8; −0.0003)	(−55.8; 0.0009)	(−30.8; −0.0001)	(−5.8; 0.0000)
		Bs	(−105.8; 0.0004)	(−89.1333; 0.0000)	(−55.8; 0.0004)	(−22.4667; 0.0000)	(−5.8; 0.0000)
	E_{ZZ}	Bz	(−105.8; −0.0001)	(−80.8; −0.0001)	(−55.8; −0.0003)	(−30.8; 0.0006)	(−5.8; 0.0002)
		Bs	(−105.8; −0.0001)	(−89.1333; −0.0001)	(−55.8; −0.0000)	(−22.4667; 0.0003)	(−5.8; 0.0002)
	E_{AZ}	Bz	(−105.8; −0.0854)	(−80.8; −0.8358)	(−55.8; −0.1734)	(−30.8; −1.5442)	(−5.8; −1.7265)
		Bs	(−105.8; −0.0899)	(−89.1333; −0.4915)	(−55.8; −0.6707)	(−22.4667; −1.5193)	(−5.8; −1.7302)
	E_{BZ}	Bz	(−105.8; −0.5004)	(−80.8; 0.4365)	(−55.8; −0.2125)	(−30.8; 0.3819)	(−5.8; 0.2103)
		Bs	(−105.8; −0.4967)	(−89.1333; 0.0422)	(−55.8; 0.0752)	(−22.4667; 0.2673)	(−5.8; 0.2168)

Table 13 Estimated control points of the Bezier (Bz) and B-spline (Bs) models for the intra-axis errors in the backward direction of the Z-axis of the Matsuura machine tool

Axis	IAEs		Control points				
			P0	P1	P2	P3	P4
Z	E_{XZ}	Bz	(−105.8; −0.0114)	(−80.8; −0.0124)	(−55.8; −0.0137)	(−30.8; −0.0152)	(−5.8; −0.0159)
		Bs	(−105.8; −0.0114)	(−89.1333; −0.0121)	(−55.8; −0.0137)	(−22.4667; −0.0154)	(−5.8; −0.0159)
	E_{YZ}	Bz	(−105.8; −0.0003)	(−80.8; 0.0005)	(−55.8; −0.0004)	(−30.8; −0.0000)	(−5.8; 0.0001)
		Bs	(−105.8; −0.0003)	(−89.1333; 0.0001)	(−55.8; −0.0001)	(−22.4667; −0.0001)	(−5.8; 0.0001)
	E_{ZZ}	Bz	(−105.8; 0.0004)	(−80.8; 0.0003)	(−55.8; 0.0001)	(−30.8; 0.0004)	(−5.8; 0.0001)
		Bs	(−105.8; 0.0004)	(−89.1333; 0.0003)	(−55.8; 0.0002)	(−22.4667; 0.0003)	(−5.8; 0.0001)
	E_{AZ}	Bz	(−105.8; 0.2994)	(−80.8; 0.6414)	(−55.8; −1.0039)	(−30.8; −0.6544)	(−5.8; −1.5193)
		Bs	(−105.8; 0.3124)	(−89.1333; 0.3938)	(−55.8; −0.5061)	(−22.4667; −1.0620)	(−5.8; −1.4955)
	E_{BZ}	Bz	(−105.8; −0.3291)	(−80.8; −0.6675)	(−55.8; 0.1214)	(−30.8; 0.5665)	(−5.8; 0.4474)
		Bs	(−105.8; −0.3260)	(−89.1333; −0.5214)	(−55.8; 0.0558)	(−22.4667; 0.4946)	(−5.8; 0.4583)

Acknowledgements The authors would like to thank Yan Boutin and Bu Khanh Vo, manufacturing engineers, for their assistance during the laboratory tests.

Author contribution AM was responsible for the literature study, data analysis, and writing the paper. MS was the supervisor of this work. He proposed the research idea, technical scheme, and all needed support conditions. He has also participated in data analysis and was responsible for completing the article. MZ was involved in the discussion and data analysis. RM and J-FC were involved in the discussion and significantly contributed to making the final draft of the article. All the authors read and approved the final manuscript.

Data availability All data presented in this paper are available.

Code availability Can be made available upon request.

Declarations

Ethics approval Not applicable.

Consent to participate All authors contribute and participate in the work carried out in this paper.

Consent for publication The authors of this paper agree to publish this work in the International Journal of Advanced Manufacturing Technology.

Competing interests The authors declare no competing interests.

References

1. Liu C, Xu X (2017) Cyber-physical machine tool – the era of machine tool 4.0. Procedia CIRP 63:70–75
2. Jeon B, Yoon JS, Um J, Suh SH (2020) The architecture development of Industry 4.0 compliant smart machine tool system (SMTS). J Intell Manuf 31:1837–1859
3. Xu X (2017) Machine Tool 4.0 for the new era of manufacturing. Int J Adv Manuf Technol 92:1893–1900
4. Rastegari A, Archenti A, Mobin M (2017) Condition based maintenance of machine tools: vibration monitoring of spindle units. Ann Reliab Maintain Symp (RAMS)
5. Fan KCh, Chen HM, Kuo TH (2012) Prediction of machining accuracy degradation of machine tools. Precis Eng Maintainability Symposium (RAMS) 36:288–298. https://doi.org/10.1109/RAM.2017.7889683
6. Gregory W, Vogl M (2016) Alkan Donmez, Andreas Archenti, Diagnostics for geometric performance of machine tool linear axes. CIRP Ann 65(1):377–380
7. de Lacalle NL, Lamikiz AL (2009) Machine tools for high performance machining. Springer, London. https://doi.org/10.1007/978-1-84800-380-4
8. Han Z, Jin H, Liu Y, Fu H (2013) A review of geometric error modeling and error detection for CNC machine tool. Appl Mech Mater 303–306:627–631. https://doi.org/10.4028/www.scientific.net/amm.303-306.627
9. Ramesh R, Mannan MA, Poo AN (2000) Error compensation in machine tools — a review Part II: thermal errors. Int J Mach Tools Manuf 40:1257–1284
10. Ramesh R, Mannan MA, Poo AN (2005) Tracking and contour error control in CNC servo systems. Int J Mach Tools Manuf 45(3):301–326
11. Lyu D, Liu Q, Liu H, Zhao W (2020) Dynamic error of CNC machine tools: a state-of-the-art review. Int J Adv Manuf Technol 106:1869–1891
12. Chen J-R, Ho B-L, Lee H-W, Pan S-P, Hsieh T-H (2018) Geometric error measurement of machine tools using autotracking laser interferometer. Sens Mater 30:2429–2435
13. Chen JS, Kou TW, Chiou SH (1999) Geometric error calibration of multi-axis machines using an auto-alignment laser interferometer. Precis Eng 23:243–252
14. Majda P (2012) Modeling of geometric errors of linear guideway and their influence on joint kinematic error in machine tools. Precis Eng 36:369–378
15. Ramesh R, Mannan M, Poo A (2000) Error compensation in machine tools—a review: part I: geometric, cutting-force induced and fixture-dependent errors. Int J Mach Tools Manuf 40:1235–1256
16. Bohez ELJ, Ariyajunya B, Sinlapeecheewa Ch, Shein TMM, Lap DT, Belforte G (2007) Systematic geometric rigid body error identification of 5-axis milling machines. Comput Aided Des 39(4):229–244

17. Khan AW, Chen W (2011) A methodology for systematic geometric error compensation in five-axis machine tools. Int J Adv Manuf Technol 53:615–628
18. Yu Z, Tiemin L, Xiaoqiang T (2011) Geometric error modeling of machine tools based on screw theory. Procedia Eng 24:845–849
19. Xing K, Achiche S, Esmaeili S, Mayer JRR (2018) Comparison of direct and indirect methods for five-axis machine tools geometric error measurement. Procedia CIRP 78:231–236
20. Slamani M, Mayer J, Cloutier G (2011) Modeling and experimental validation of machine tool motion errors using degree optimized polynomial including motion hysteresis. Exp Tech 35:37–44
21. Lee JH, Liu Y, Yang S-H (2006) Accuracy improvement of miniaturized machine tool: Geometric error modeling and compensation. Int J Mach Tools Manuf 46:1508–1516
22. Slamani M, Mayer R, Balazinski M (2013) Concept for the integration of geometric and servo dynamic errors for predicting volumetric errors in five-axis high-speed machine tools: an application on a XYC three-axis motion trajectory using programmed end point constraint measurements. Int J Adv Manuf Technol 65:1669–1679
23. Slamani M, Mayer R, Balazinski M, Zargarbashi SHH, Engin S, Lartigue C (2010) Dynamic and geometric error assessment of an XYC axis subset on five-axis high-speed machine tools using programmed end point constraint measurements. Int J Adv Manuf Technol 50:1063–1073
24. Aguado S, Samper D, Santolaria J, Aguilar JJ (2012) Identification strategy of error parameter in volumetric error compensation of machine tool based on laser tracker measurements. Int J Mach Tools Manuf 53:160–169
25. Qianjian G, Jianguo Y (2011) Application of projection pursuit regression to thermal error modeling of a CNC machine tool. Int J Adv Manuf Technol 55:623–629
26. Lin J, Zhang Y, Zhang X, Li W, Lin W (2018) Parametric modeling of geometric errors for CNC machine tools based on Chebyshev polynomial. In (2018) IEEE 3rd Advanced Information Technology, Electronic and Automation Control Conference (IAEAC) 2293–2297
27. Peng W, Xia H, Wang S, Chen X (2018) Measurement and identification of geometric errors of translational axis based on sensitivity analysis for ultra-precision machine tools. The International Journal of Advanced Manufacturing Technology 94:2905–2917
28. Lasemi A, Xue D, Gu P (2016) Accurate identification and compensation of geometric errors of 5-axis CNC machine tools using double ball bar. Meas Sci Technol 27(5)
29. Qiao Z, Hu M, Tan Z, Liu Z, Liu L, Hu W (2019) An accurate and fast method for computing offsets of high degree rational Bézier/NURBS curves with user-definable tolerance. J Comput Lang 52:1–9
30. Jin Y, Zhao S, Wang Y (2019) An optimal feed interpolator based on G 2 continuous Bézier curves for high-speed machining of linear tool path. Chin J Mech Eng 32:1–10
31. Bruni C, Mancia T, Greco L, Pieralisi M (2020) Additive manufacturing using UV polymerization of complex surfaces generated by two main B-splines. Procedia Manuf 47:1078–1083
32. Lin F, Shen L-Y, Yuan C-M, Mi Z (2019) Certified space curve fitting and trajectory planning for CNC machining with cubic B-splines. Comput Aided Des 106:13–29
33. Li J, Wang Q, Zhong G (2020) Planar tool radius compensation for CNC systems based on NURBS interpolation. Mech Ind 21:107
34. Msaddek EB, Bouaziz Z, Baili M, Dessein G, Akrout M (2017) Simulation of machining errors of Bspline and Cspline. Int J Adv Manuf Technol 89:3323–3330
35. De Santiago-Perez JJ, Osornio-Rios RA, Romero-Troncoso R, Morales-Velazquez L (2013) FPGA-based hardware CNC interpolator of Bezier, splines, B-splines and NURBS curves for industrial applications. Comput Ind Eng 66:925–932
36. Khan AW, Chen WA (2011) Methodology for systematic geometric error compensation in five-axis machine tools. Int J Adv Manuf Technol 53:615–628. https://doi.org/10.1007/s00170-010-2848-3
37. Bartoň M, Bizzarri M, Rist F, Sliusarenko O, Pottmann H (2021) Geometry and tool motion planning for curvature adapted CNC machining. ACM Trans Graph 40(4):1–16. https://doi.org/10.1145/3450626.3459837
38. Lartigue C, Tournier C, Ritou M, Dumur D (2004) High-performance NC for HSM by means of polynomial trajectories. Ann CIRP 53(1):317–320
39. Calleja A, Bo P, González H, Barton M, López de Lacalle LN (2018) Highly accurate 5-axis flank CNC machining with conical tools. Int J Adv Manuf Technol 97:1605–1615. https://doi.org/10.1007/s00170-018-2033-7
40. Erik LJ (2007) Bohez, Bancha Ariyajunya, Chanin Sinlapeecheewa, Tin Maung Maung Shein, Do Tien Lap, Gustavo Belforte, Systematic geometric rigid body error identification of 5-axis milling machines. Comput Aided Des 39(4):229–244
41. Wu B, Yin Y, Zhang Y, Luo M (2019) A new approach to geometric error modeling and compensation for a three-axis machine tool. Int J Adv Manuf Technol 102:1249–1256
42. Ekinci TO, Mayer JRR (2007) Relationships between straightness and angular kinematic errors in machines. Int J Mach Tools Manuf 47(12–13):1997–2004
43. Tang H, Duan J-A, Zhao Q (2017) A systematic approach on analyzing the relationship between straightness & angular errors and guideway surface in precise linear stage. Int J Mach Tools Manuf 120:12–19
44. Florussen GHJ, Delbressine FLM, Van de Molengraft MJG, Schellekens PHJ (2001) Assessing geometrical errors of multi-axis machines by three-dimensional length measurements. Measurement 30(4):241–255
45. Lou ZF, Fan. KC (2019) Optical sensors for machine tool metrology. In: Gao W. (eds) Metrology. Precis Manuf. Springer, Singapore. https://doi.org/10.1007/978-981-10-4912-5_4-1
46. Farin G (2006) Class a Bézier curves. Computer Aided Geometric Design 23:573–581
47. Borges CF, Pastva T (2002) Total least squares fitting of Bézier and B-spline curves to ordered data. Comput Aided Geomet Des 19:275–289
48. ISO 230–2 (1997) Test code for machine tools—Part 2: determination of accuracy and repeatability of positioning of numerically controlled axes. International Organization for Standardization, Geneva
49. Cai C, Wang G, Wen Y, Pei J, Zhu X, Zhuang W (2010) Superconducting transition temperature T c estimation for superconductors of the doped MgB 2 system using topological index via support vector regression. J Supercond Novel Magn 23:745–748
50. Taylor R (1990) Interpretation of the correlation coefficient: a basic review. J Diagn Med Sonogr 6:35–39
51. Duncan M (2005) Bézier Curves II. In applied geometry for computer graphics and CAD Springer, London. https://doi.org/10.1007/1-84628-109-1_7
52. Piegl LA, Tiller W (1997) The NURBS book. Springer, Berlin